Authors version; accepted for publication in Journal of Computational Science on April 23, 2017

Modeling regulation of vascular tone following muscle contraction: model development, validation and global sensitivity analysis

J.M.T. Keijsers[1,2,*], *C.A.D. Leguy*[2], *A.J. Narracott*[3,4], *J. Rittweger*[2], *F.N. van de Vosse*[1] *and W. Huberts*[5]

[1] Department of Biomedical Engineering, Eindhoven University of Technology, Eindhoven, The Netherlands [2] Institute of Aerospace Medicine, German Aerospace Center, Cologne, Germany [3] Medical Physics Group, Department of Cardiovascular Science, University of Sheffield, Sheffield, United Kingdom [4] INSIGNEO Institute for *in silico* Medicine, University of Sheffield, Sheffield, United Kingdom [5] Department of Biomedical Engineering, Maastricht University, Maastricht, The Netherlands

ABSTRACT

In this study the regulation of vascular tone inducing the blood flow increase at the onset of exercise is examined. Therefore, our calf circulation model was extended with a regulation model to simulate changes in vascular tone depending on myogenic, metabolic and baroreflex regulation. The simulated blood flow corresponded to the in vivo response and it was concluded that metabolic activation caused the flow increase shortly after muscle contraction. Secondly, the change in baseline flow upon tilt was a result of myogenic and baroreflex activation. Based on a sensitivity analysis the myogenic gain was identified as most important parameter.

Keywords: regulation of vascular tone, metabolic regulation, myogenic regulation, baroreflex, 1D pulse wave propagation.

Corresponding address: J.M.T. Keijsers, Department of Biomedical Engineering. Eindhoven University of Technology, PO Box 513, 5600 MB, Eindhoven. The Netherlands. Phone: +3140 247 5675. Email: j.m.t.keijsers@tue.nl

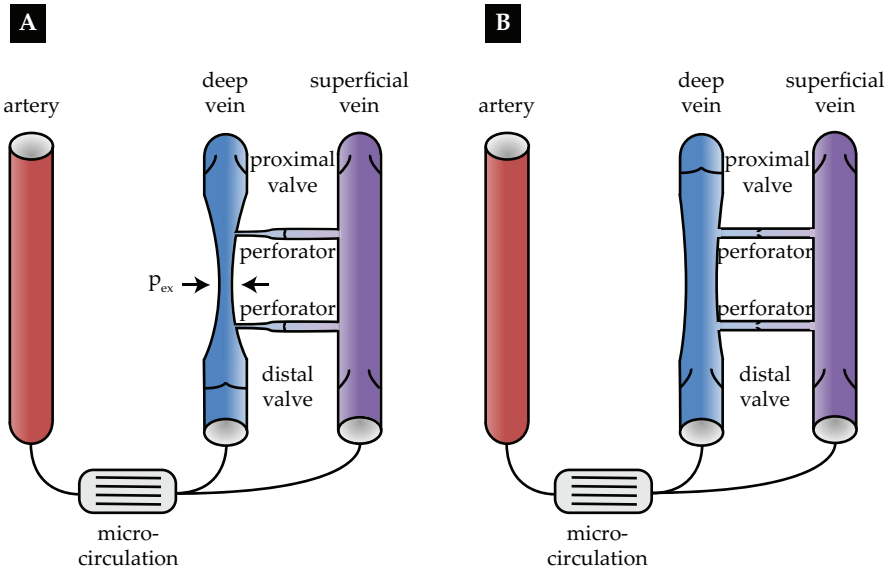

Figure 1: Schematic representation of the muscle pump effect during the **A** contraction and **B** relaxation phase. During contraction, the deep vein collapses due to the extravascular pressure p_{ex} exceeds the intravascular pressure. Venous return is increased, whereas back-flow and flow to the superficial system is blocked by the distal and perforator valves. During the relaxation, the deep vein is refilled from both the artery and the superficial vein, while the perforator valves open and the proximal valve is closed to prevent back-flow. Figure was adapted from Keijsers et al. [2015]

1 Introduction

During exercise several complex haemodynamic regulation mechanisms are activated to ensure sufficient supply of oxygen and nutrients, and removal of waste products. Increased understanding of these individual mechanisms and their interaction is needed to fully characterize the dynamics of blood flow during exercise. At the onset of exercise, the blood flow within muscle in the lower limb increases significantly depending on the arterio-venous pressure drop and the peripheral resistance. These are influenced by both mechanical effects during muscle contraction and relaxation (the muscle pump effect) and the vasodilatory state of the arterioles. However, the exact contribution of these two mechanisms to the blood flow increment at the onset of exercise is still a matter of debate [Tschakovsky and Sheriff, 2004]. Three hypotheses are currently described in literature: the first states that flow augmentation is primarily caused by the muscle pump effect, the second claims that regulation of peripheral resistance is the major determinant. The third hypothesis considers both mechanisms to be important.

As a result of calf muscle activation, the muscle pump effect increases venous return by collapsing the deep veins embedded within the muscle. Furthermore, backflow towards the arterial system and into the superficial venous system is prevented by closure of the distal and perforating venous valves respectively (Figure 1A) [Rowell, 1993]. Arterial inflow rises during subsequent muscle relaxation as the perfusion pressure is increased due to the pressure shielding of the closed proximal valve (Figure 1B) [Rowell, 1993]. Furthermore, the opening of the distal and perforating valves [Meissner, 2005] allows venous refilling from both the arterial and superficial venous system. In summary, the muscle pump effect increases blood flow through an increase in arterio-venous pressure drop.

In a previous study [Keijsers et al., 2015], we examined the role of venous valves, hydrostatic pressure and the superficial veins during the muscle pump using a mathematical

model. Although the model was able to simulate the increased venous return during muscle contraction and the elevated arterial flow during muscle relaxation, the predicted flow augmentation was low compared to the increase in arterial flow increase measured during *in vivo* calf muscle contractions [Nådland et al., 2009]. Based on the debate in literature [Nådland et al., 2009, Tschakovsky et al., 1996], it was proposed that vasodilation could be the missing component in the model. Furthermore, the simulated arterial baseline flow in the tilted position was equal to the baseline flow in the supine position, which was in strong contrast with the 50% decay observed *in vivo* [Nådland et al., 2009]. These postural changes can be attributed to changes in peripheral resistance due to myogenic vasoconstriction and a global increase in peripheral resistance [Nådland et al., 2009]. Therefore, in this study our previous model is extended to include regulation of vascular tone.

Regulation of vascular tone in skeletal muscle tissue is not based on a single mechanism, but involves the interaction between the local myogenic, local metabolic and global baroreflex regulation [Joyner and Casey, 2015]. Myogenic regulation protects the capillaries against high pressures by vasoconstriction as transmural pressure increases [Boron and Boulpaep, 2003]. The metabolic mechanism induces vasodilation when the amount of metabolites accumulates, thereby regulating the oxygen delivery and removal of waste products [Boron and Boulpaep, 2003, Joyner and Casey, 2015]. Finally, the baroreflex initiates vasoconstriction when central pressure detected by the baroreceptors in the aortic arch and the carotid artery decreases. In addition, the baroreflex affects heart rate, cardiac contractility and venous unstressed volume [Boron and Boulpaep, 2003, Rowell, 1993]. A combined regulation model including all three components is thus required to describe the resulting vascular tone. As all three mechanisms respond to different parameters and with different time delays, each should be modelled as a separate component. The definition of specific parameters for each mechanism, allows us to examine the relative activation of the three mechanisms during muscle contraction and relaxation.

Previous numerical studies of regulation of vascular tone have focussed on cerebral auto-regulation or the baroreflex. Ursino [1988] developed a model for cerebral auto-regulation including a neurogenic and endothelial response in addition to the myogenic and metabolic mechanism. This model was used to investigate the relation between cerebral blood volume and intracranial pressure changes [Ursino and Giammarco, 1991] and applied to examine cerebral regulation under squat exercise and visual stimulation [Spronck et al., 2012]. Models of the baroreflex have been applied to study various physiological responses, e.g. the interaction between the baroreflex and a pulsating heart model [Ursino, 1998], heart rate variability [Ursino and Magosso, 2003], fetal welfare during labor [van der Hout-van der Ja 2013] and heart rate regulation under orthostatic stress [Olufsen et al., 2006]. However, to our knowledge, no model exists that combines myogenic, metabolic and baroreflex regulation to simulate the vascular tone response to a skeletal muscle contraction.

The aim of this study was to determine the importance of the myogenic, metabolic and baroreflex regulation during the different phases of muscle contraction. Therefore, the 1D arterio-venous model as described in Keijsers et al. [2015] was extended with a regulation model for the vascular tone, which includes both the myogenic and metabolic effects described by Spronck et al. [2012], combined with the baroreflex model of Ursino [1998] to include all three mechanisms. In an initial explorative analysis, the intuitively most important model parameters representing the gain of the myogenic and metabolic mechanism were fitted to match the measured *in vivo* flow response to a muscle contraction in the supine position. Secondly, the same parameters were used to predict the response to a muscle contraction in the tilted position. Finally, a sensitivity analysis was performed to quantify which parameters are most important for the variance in the flow response. For the sensitivity analysis the two step approach as described by Donders et al. [2015]

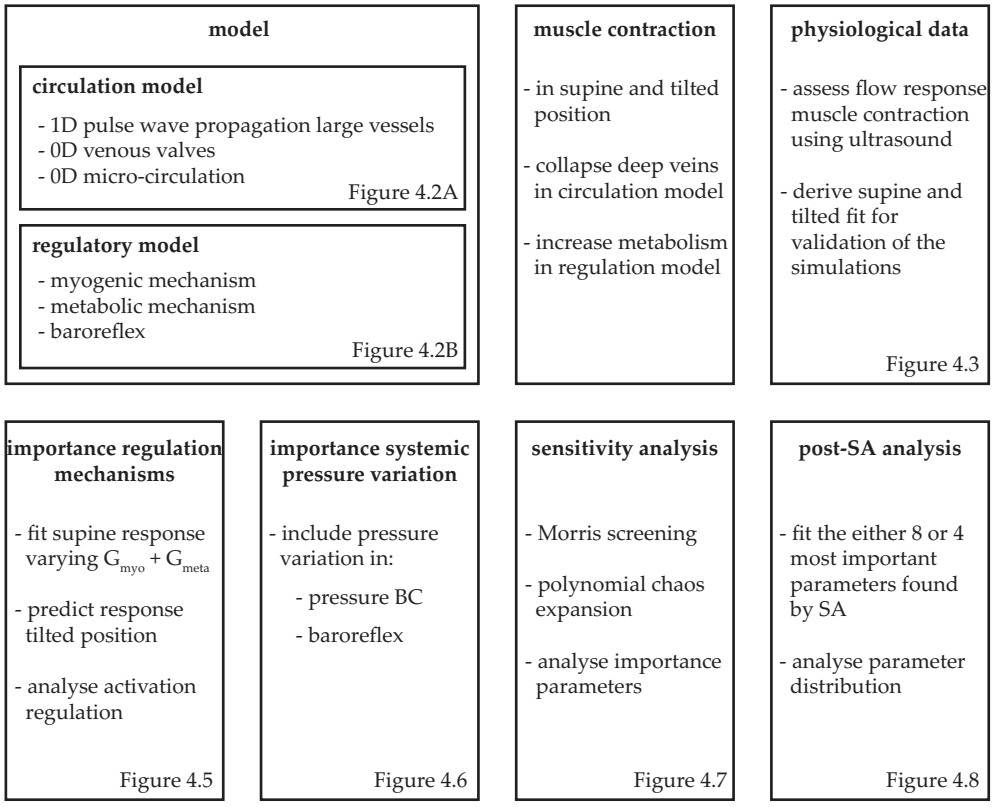

Figure 2: Schematic overview of the methods as described in this study including: circulatory and regulation model, simulation of a muscle contraction, physiological data, and the four analyses performed. For each part the main points are given together with the corresponding figures.

was used. This approach consists of an initial Morris screening and a subsequent generalized polynomial chaos expansion (gPCE). We conclude with an analysis varying the most important parameters, identified by the sensitivity analysis, to fit the *in vivo* response.

2 Methods

In this section the methods are described and a schematic overview can be observed in Figure 2.

2.1 Model

To study the hemodynamic and local regulatory response to muscle contraction in the lower limb a simplified model of the calf circulation was constructed (Figure 3). The model includes an artery, supplying the muscle tissue with oxygen, a deep vein, embedded in the muscle tissue, and a superficial vein, between the skin and the muscle. To model regulation of vascular tone the mean response of the arterioles is included into a single model variable which represents the regulatory state. This state is based on the myogenic, metabolic and baroreflex regulation (Figure 3B). Changes in peripheral resistance are induced by relating the resistance to the regulation state. The following section describes the physiological background and governing equations of the various model components.

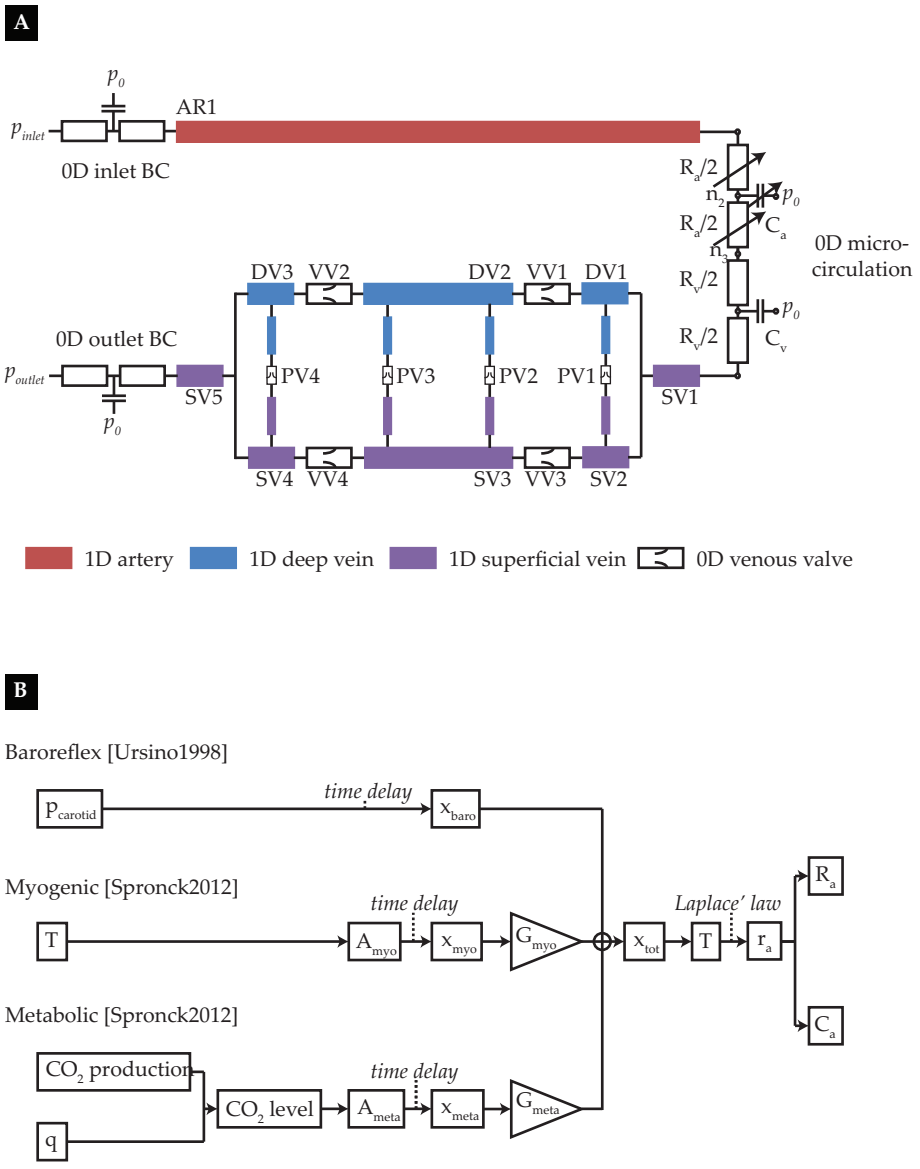

Figure 3: Model. **A** Model configuration of the calf circulation including: 1D artery (AR), a 1D deep (DV) and superficial (SV) vein, 0D venous valves (VV), a 0D micro-circulation, a 0D inlet and outlet boundary condition (BC). The length and radius of the 1D elements are not true to scale (geometrical parameters of all 1D segments can be found in Table 1) **B** Schematic overview of the regulation model including baroreflex, myogenic and metabolic regulation

2.1.1 1D Pulse wave propagation: arteries and veins

The hemodynamics in the large arteries and veins is captured using the 1D equations for mass and momentum balance, with blood assumed to be an incompressible Newtonian fluid. The resulting equations read:

$$C\frac{\partial p_{\text{tr}}}{\partial t} + \frac{\partial q}{\partial z} = 0, \tag{1}$$

$$\frac{\partial q}{\partial t} + \frac{\partial A\overline{v_z^2}}{\partial z} + \frac{A}{\rho}\frac{\partial p}{\partial z} = \frac{2\pi a}{\rho}\tau_w + Ag_z, \tag{2}$$

where C is the compliance per unit length, $p_{\text{tr}} = p - p_{\text{ex}}$ is the transmural pressure, p and p_{ex} are the intra- and extravascular pressure respectively, q is the flow, t is the time and z is the axial coordinate. Furthermore, A is the cross-sectional area, $\overline{v}_z$ is the velocity in axial direction averaged over the cross-sectional area, ρ is blood fluid density, $a = \sqrt{A/\pi}$ is the radius and τ_w is the wall shear stress. Additionally, $g_z = g\ \mathbf{e_g} \cdot \mathbf{e_z}$ is the contribution of the gravitational acceleration in the axial direction, g is the magnitude of the gravitational acceleration on earth, $\mathbf{e_g}$ is the unit vector in the direction of gravity and $\mathbf{e_z}$ is the unit vector in axial direction.
To obtain an estimation of the wall shear stress τ_w and the advection term $\frac{\partial A\overline{v_z^2}}{\partial z}$ the approximate velocity profile is used (see Bessems et al. [2007] for more details). Here, the pressure gradient and the gravitational forces are assumed to be in balance with viscous forces in the boundary layer close to the vessel wall. In the central core inertia forces are assumed to be in balance with the pressure gradient and the gravitational forces. Finally, a constitutive law relating cross-sectional area and pressure, is defined for both arteries and veins.
As the arterial cross-sectional area variations during the cardiac cycle are small under normal conditions, the mechanical characteristics of the arterial wall are modeled with the following linear A, p relation

$$A = A_{\text{ref,A}} + C(p_{\text{tr}} - p_{\text{ref,A}}), \tag{3}$$

where $A_{\text{ref,A}}$ is the reference cross-sectional area at reference pressure $p_{\text{ref,A}}$ and C the linearized compliance per unit length at reference pressure $p_{\text{ref,A}}$. The compliance is determined using thin-walled-cylinder theory for a linear isotropic elastic material:

$$C = \left.\frac{\partial A}{\partial p_{\text{tr}}}\right|_{p_{\text{tr}}=p_{\text{ref,A}}} = \frac{2\pi(1-\nu^2)r_{\text{ref,A}}^3}{hE}\ , \tag{4}$$

where ν is the Poisson's ratio, $r_{\text{ref,A}} = \sqrt{A_{\text{ref,A}}/\pi}$ is the reference radius, $h \approx r_{\text{ref,A}}/10$ is the vessel wall-thickness [Westerhof et al., 1969] and E is the Young's modulus.
Because veins are prone to collapse under low transmural pressures due to e.g. increasing extravascular pressure during muscle contraction or gravitational stress, a nonlinear pressure area relationship needs to be considered. Therefore, Shapiro [1977] derived a tube law capturing the venous collapse with an p, A-relation. In order to solve the full system of equations for pressure a fit of the tube law is used as derived in Keijsers et al. [2015].

$$A = A_{\text{ref,V}}\left\{h(p^*)f^+(p^*) + (1-h(p^*))f^-(p^*)\right\}, \tag{5}$$

where $A_{\text{ref,V}}$ is the reference cross-sectional area at zero transmural pressure, $p^* = p_{\text{tr}}/K_p$ is the dimensionless pressure and K_p is the bending stiffness. The functions f^+ and f^- are fits of the positive and negative pressure part of the original tube law of Shapiro and

Table 1: Geometrical parameters of the various 1D vessels [Müller and Toro, 2014] as depicted in Figure 3. The four perforating veins consist of a deep (PV#-D) and a superficial (PV#-S) vein of which the parameters are noted separately.

Vessel	Numbering (Figure 3)	Radius [mm]	Length [cm]
artery	AR1	2.5	34
deep vein	DV1	1.5	2
	DV2	1.5	26
	DV3	1.5	2
superficial vein	SV1	3.5	2
	SV2	1.5	2
	SV3	1.5	26
	SV4	1.5	2
	SV5	3.5	2
perforating vein	PV#-S	0.5	1.5
	PV#-D	0.5	1.5

$h(p^*)$ is a scaling function.

$$f^+(p^*) = \frac{A_0^+}{\pi}\left(\tan^{-1}\left(\frac{p^*-p_a^+}{p_b^+}\right)+\frac{\pi}{2}\right), \tag{6}$$

$$f^-(p^*) = B+\frac{A_0^-}{\pi}\left(\tan^{-1}\left(\frac{p^*-p_a^-}{p_b^-}\right)+\frac{\pi}{2}\right), \tag{7}$$

$$\text{and} \qquad h(p^*) = \frac{1}{\pi}\left(\tan^{-1}\left(\frac{\gamma p^*}{\pi}\right)+\frac{\pi}{2}\right), \tag{8}$$

where B, A_0^-, p_a^-, p_b^-, A_0^+, p_a^+, p_b^+ and γ are fitting constants determining the shape of the A,p-relation. Venous compliance is calculated as the derivative of cross-sectional area with respect to the transmural pressure.

2.1.2 0D Venous valves

The pressure-flow relation of a venous valve is included using the versatile valve model of Mynard et al. [2012]. As the flow through venous valves is much lower compared to heart valves, the linear viscous forces are included, as in Keijsers et al. [2016].

$$\Delta p = Rq + Bq|q| + L\frac{\partial q}{\partial t}, \tag{9}$$

where the Poiseuille resistance R, Bernouilli resistance B and the inertance L are defined by

$$R = \frac{8\pi\eta l_{\text{eff}}}{A_{\text{eff}}^2}, \qquad B = \frac{\rho}{2A_{\text{eff}}^2} \qquad \text{and} \qquad L = \frac{\rho l_{\text{eff}}}{A_{\text{eff}}}, \tag{10}$$

where A_{eff} is the effective cross-sectional area, η is the dynamic blood viscosity, and $l_{\text{eff}} = \beta_l \cdot r_{\text{ref,V}}$ is the effective valve length defined as a multiple β_l of the venous reference radius $r_{\text{ref,V}} = \sqrt{A_{\text{ref,V}}/\pi}$ [Keijsers et al., 2016]. To include valve opening and closing, the effective cross-sectional area is defined to be a function of valve state ζ via the following relation

$$A_{\text{eff}} = (A_{\text{eff,max}} - A_{\text{eff,min}})\,\zeta + A_{\text{eff,min}}, \tag{11}$$

where $A_{\text{eff,min}}$ and $A_{\text{eff,max}}$ are the minimal and maximal effective cross-sectional area respectively. Here, maximal effective cross-sectional area $A_{\text{eff,max}} = \beta_A \cdot A_{\text{ref,V}}$ is defined as a multiple β_A of the reference cross-sectional area $A_{\text{ref,V}}$ of the connecting vein. The valve state is defined to vary between zero and one (fully closed: $\zeta = 0$, fully open:

$\zeta = 1$). Its value is related via two differential equations for valve opening and closing respectively:

$$\frac{d\zeta}{dt} = \begin{cases} (1-\zeta)\, K_{\text{vo}}\, (\Delta p - dp_{\text{valve},0})\,, & \text{if } \Delta p > dp_{\text{valve},0} \\ \zeta K_{\text{vc}}\, (\Delta p - dp_{\text{valve},0})\,, & \text{if } \Delta p < dp_{\text{valve},0} \end{cases}, \tag{12}$$

where K_{vo} and K_{vc} are coefficients determining the opening and closing speed of the valve. Furthermore, $dp_{\text{valve},0}$ is the pressure drop above and below which opening and closing is initiated.

2.1.3 0D micro-circulation

To account for the pressure drop over the micro-circulation (in the current study defined to include the arterioles, capillaries and venules) and its storage capacity, the micro-circulation model consists of both resistances and compliances. The micro-circulation is split into an arteriolar and venular part, both consisting of two resistances R_{i} ($i = a, v$) in series and a compliance C_{i} ($i = a, v$) connected to the extravascular pressure, for which the following relations hold (Figure 3A).

$$\Delta p = R_{\text{i}} q \qquad \text{and} \qquad \frac{\partial p_{tr}}{\partial t} = \frac{1}{C_{\text{i}}} q. \tag{13}$$

Under baseline conditions the total resistance of the two parts is determined by the pressure drop over the micro-circulation Δp_{bl} and the time-avaraged baseline flow $\overline{q_{\text{bl}}}$ according to

$$R_{\text{tot}} = \frac{\Delta p_{\text{bl}}}{\overline{q_{\text{bl}}}} = R_{\text{a}} + R_{\text{v}}, \tag{14}$$

where R_{v} is chosen such that the pressure drop over the venules is 400 Pa [Boron and Boulpaep, 2003]. Furthermore the baseline total compliance C_{tot} is derived from a typical time-constant τ_{RC} as in a classical single windkessel micro-circulation [Keijsers et al., 2015]. The compliance of the venules is assumed to be much larger than arteriolar compliance [Boron and Boulpaep, 2003]. Therefore, the compliances are distributed as follows

$$C_{\text{a}} = 0.3 \cdot C_{\text{tot}} \qquad \text{and} \qquad C_{\text{v}} = 0.7 \cdot C_{\text{tot}}. \tag{15}$$

The above equations for resistance and compliance relate to the baseline conditions. However, for the arteriolar part of the micro-circulation the resistance and compliance are regulated by vascular tone as described in the following subsection.

2.1.4 Regulation of vascular tone

Regulation of the vascular tone in muscular tissue is based on the following mechanisms (Figure 3B):

- Myogenic regulation: protecting the capillaries against excessive pressures
- Metabolic regulation: matching the blood flow to the oxygen demand
- Baroreflex regulation: aiming to maintain the level of systemic pressure

The regulation model is based on the implementation of cerebral auto-regulation as described by Spronck et al. [2012]. In this study, each regulation mechanisms is included individually and represented by a regulatory state x_i. The myogenic regulatory state x_{myo} is derived from the arteriolar wall tension T and has a time constant τ_{myo}. The metabolic regulatory state x_{meta} with time constant τ_{meta} is modeled to depend on tissue CO_2-level,

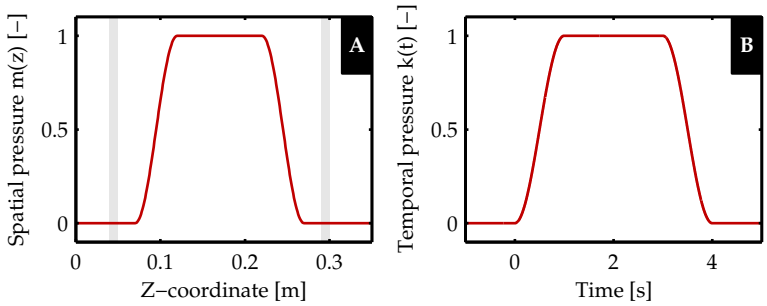

Figure 4: Extravascular pressure of the deep veins is increased to simulate a muscle contraction. Plot **A** and **B** show the spatial $m(z)$ and temporal $k(t)$ course of extravascular pressure as applied to the deep venous elements respectively (see Appendix A for the full equations of $m(z)$ and $k(t)$). The grey areas in the spatial plot indicate the location of the venous valves. [Keijsers et al., 2015]

which is derived from the CO_2-production and the blood flow. The latter two regulatory mechanism are included as described by Spronck et al. [2012], but the metabolic mechanism is adjusted to induce metabolic activation upon muscle contraction instead of cerebral activity, as included by Spronck et al. [2012]. Furthermore, tissue specific parameters are updated to match muscle tissue. Finally, the baroreflex regulatory state x_{baro} is based on the carotid pressure, which is derived from the pressure at the heart level based on the hydrostatic column. The baroreflex implementation is based on the model based on the study of Ursino [1998]. The total regulatory state is calculated as the weighted sum of the three mechanisms, each having a specific gain: G_{myo}, G_{meta} and G_{baro}. The total regulatory state is translated to arteriolar wall tension, which is subsequently converted to the arteriolar radius using Laplace's law. Finally, the arteriolar radius is used to determine the change in peripheral resistance and compliance. For completeness, the equations describing the activation of the three regulation mechanisms and how they affect a change in resistance and compliance are given in Appendix B.

2.1.5 Boundary conditions

Both the inlet of the 1D arterial and the outlet of the 1D venous part are connected to a three element windkessel model representing the proximal vasculature. Each windkessel element consists of two resistances in series and a compliance connected to the extravascular pressure p_0 (Equation (13)). The total windkessel resistance is the sum of the Poiseuille resistances of the proximal vasculature, based on the geometrical parameters of the arterial and venous tree published by Müller and Toro [2014]. Similarly, the inlet and outlet compliance is the sum of the compliances of the proximal vasculature based on Equation (4) and the derivative of Equation (5) times the length respectively. At the inlet and outlet the pressure is set to a time-averaged p_{inlet} and p_{outlet} respectively. When a head up tilt position is simulated the hydrostatic column up to the heart is added to both the inlet and outlet pressure.
The model formulation described above is completed for the current application by defining the form of the muscle contraction.

2.1.6 Simulating muscle contraction

The effect of a muscle contraction is included in the current model both in a mechanical and a metabolic manner. The mechanical effect on the deep veins is expected to be large due to their location, embedded in the muscle tissue, and the low intravascular pres-

sure. Similar to Keijsers et al. [2015], a muscle contraction is simulated by an increase in extravascular pressure included in the equation for mass balance and the venous constitutive law (Equation (1) and (5) respectively). The extravascular pressure is defined by the following relation

$$p_{\text{ex}} = p_{\text{ex,max}} \cdot k(t) \cdot m(z), \tag{16}$$

where $p_{\text{ex,max}}$ is the maximal extravascular pressure, and $k(t)$ and $m(z)$ are the temporal and spatial course of extravascular pressure, respectively. The latter can be observed in Figure 4, and the full equations are give in Appendix A. The influence of the muscle contraction on the superficial veins is assumed to be negligible due to their location outside the muscle tissue. Furthermore, due to the high arterial pressure the influence of the muscle contraction on the arterial cross-sectional area is also assumed to be negligible. Finally, the mechanical influence on the micro-circulation is also assumed to be negligible due to its viscous character (in Equation (13) and (24)) [Gray et al., 1967]. Although contradicted in some studies [Tschakovsky et al., 1996], few experimental studies hypothesize the decrease in transmural pressure could induce myogenic vasodilation [Tschakovsky and Sheriff, 2004], but implementation of this theory requires more accurate knowledge of the magnitude of extravascular pressure and is therefore neglected.
The increase in metabolism due to a muscle contraction is included in the metabolic mechanism of the regulation of vascular tone via muscle activation A_{mc} (Equation (37)). Because the flow increase due to a muscle contraction increases linearly with increasing contraction intensity [Tschakovsky et al., 2004], muscle activation is defined to follow the contraction pattern defined by the extravascular pressure and reaches a maximum of $A_{\text{mc,max}}$ corresponding to the percentage of maximum electromyogram (EMG) activity:

$$A_{\text{mc}} = A_{\text{mc,max}} \cdot k(t). \tag{17}$$

2.1.7 Numerical implementation

The model equations were implemented in the finite element package SEPRAN (Ingenieursbureau SEPRA, Leidschendam, the Netherlands) using the computational method described by Kroon et al. [2012]. Time discretization was included based on an implicit Euler scheme with a time step of $\Delta t = 1.0$ ms and spatial discretization based on the trapezium rule with element size $\Delta z = 1.0$ cm for arterial and superficial venous segments, and $\Delta z = 0.5$ cm for the deep venous segments, which is necessary to capture the collapse accurately. The model parameters that are not included in the sensitivity analysis are summarized in Table 2. Pre- and post-processing was performed using MATLAB R2012b (MathWorks, Natick, MA, USA).

2.2 Physiological data

Pressure and flow measurements were performed on twelve healthy subjects (29 ± 3 years, six male, six female, BMI: 23.4 ± 2.3 kg m^{-2}) during muscle contraction in both the supine and 70° head up tilt positions. These experiments were approved by the ethical committee of the Northern Rhine Medical Association, Germany (*Ethikkommission der Ärztekammer Nordrhein*). Subjects were asked to perform a contraction of the left calf muscle corresponding to 30% of maximal electromyography (EMG) activity (Ambu Blue Sensor N, Ballerup, Denmark). Visual feedback of the relative muscle activity was provided to enable the subjects to maintain muscle activity at the prescribed level. During the experiment blood pressure waveforms were measured at the finger using photoplethysmography (Finometer Midi, AD instruments), while maintaining the wrist at heart level. Furthermore, femoral artery blood flow was assessed using a Mylab 25 ultrasound scanner (Esaote, the Netherlands) equipped with a linear array probe and having a center

Table 2: Constant model parameters

Symbol	Value	Unit	Description
ρ	1050	kg m^{-3}	Blood mass density [Kenner, 1989]
g	9.81	m s^{-1}	Gravitational acceleration
$p_{\text{ref,A}}$	13	kPa	Arterial reference pressure [Bessems et al., 2007]
ν	0.5	-	Poisson's ratio [Westerhof et al., 1969]
E	1.6	MPa	Arterial Young's modulus [Westerhof et al., 1969]
K_p	425	Pa	Bending stiffness [Müller and Toro, 2014]
A_0^+	1.37	-	Fitting constant [Keijsers et al., 2015]
p_a^+	-2.53	-	Fitting constant [Keijsers et al., 2015]
p_b^+	3.02	-	Fitting constant [Keijsers et al., 2015]
B	0.108	-	Fitting constant [Keijsers et al., 2015]
A_0^-	1.28	-	Fitting constant [Keijsers et al., 2015]
p_a^-	-1.49	-	Fitting constant [Keijsers et al., 2015]
p_b^-	2.03	-	Fitting constant [Keijsers et al., 2015]
γ	4	-	Fitting constant [Keijsers et al., 2015]
η	4.5	mPa s	Dynamic blood viscosity [Letcher et al., 1981]
β_l	1.0	-	Effective valve length ratio [Keijsers et al., 2016]
$A_{\text{eff,min}}$	1.0	10^{-20} m^2	Minimal effective valve cross-sectional area [Mynard et al., 2012]
β_A	0.65	-	Effective valve cross-sectional area ratio [Keijsers et al., 2016]
K_{vo}	0.3	Pa^{-1}s^{-1}	Valve opening constant [Mynard et al., 2012]
K_{vc}	0.3	Pa^{-1}s^{-1}	Valve closing constant [Mynard et al., 2012]
$dp_{\text{valve,0}}$	0	Pa	Valve opening and closing pressure drop [Keijsers et al., 2016]
τ_{RC}	2.0	s	Typical time constant for windkessel element [Keijsers et al., 2016]
$p_{\text{ex,max}}$	20	kPa	Maximal extravascular pressure [Keijsers et al., 2016]

frequency of 10 MHz. The blood flow measurement were performed in pulsed-Doppler mode. Blood flow was estimated from mean blood flow velocity and vessel diameter using the Poiseuille formulation [Leguy et al., 2009].
To use the experimental data for validation of the simulated muscle flow, the *in vivo* flow decay after muscle contraction ($10 \text{ s} < t < 50$ s) was captured using the following exponential decay relation and a non-linear least squares fit.

$$q_{\text{fit}}(t) = q_0 + (q_{\text{max}} - q_0)e^{-(t-t_{\text{max}})/\tau}, \tag{18}$$

where $t_{\text{max}} = 10$ s, q_0 is the baseline flow, q_{max} is the flow at $t = t_{\text{max}}$ and τ is the time constant of the flow decay. Measurements are excluded from postprocessing when (1) average arterial pressure is below 50 mmHg for a whole experiment, (2) femoral artery flow was only measured successful during part of the experiment or (3) the quality of the flow fit was too low ($R^2_{\text{adj}} < 0.6$). An average of the pressure and femoral artery flow was derived in the supine and head up tilt positions using the following relation

$$\overline{\overline{x}}(t) = \frac{1}{N_{\text{subj}}} \sum_{\text{i}_{\text{subj}}}^{N_{\text{subj}}} \frac{1}{N_{\text{MC,i}_{\text{subj}}}} \sum_{i_{\text{MC}}}^{N_{\text{MC,i}_{\text{subj}}}} x_{\text{i}_{\text{subj}},\text{i}_{\text{MC}}}(t), \tag{19}$$

where N_{subj} is the number of subjects, $N_{\text{MC,i}_{\text{subj}}}$ is the number of muscle contractions performed by subject i_{subj} and $x_{\text{i}_{\text{subj}},\text{i}_{\text{MC}}}(t)$ is the waveform obtained during muscle contraction i_{MC} of subject i_{subj}. The corresponding intersubject standard deviation was derived using the following relation:

$$\sigma^2(t) = \frac{1}{N_{\text{subj}} - 1} \sum_{\text{i}_{\text{subj}}}^{N_{\text{subj}}} \left(\overline{x}_{\text{i}_{\text{subj}}} - \overline{\overline{x}}(t) \right)^2, \tag{20}$$

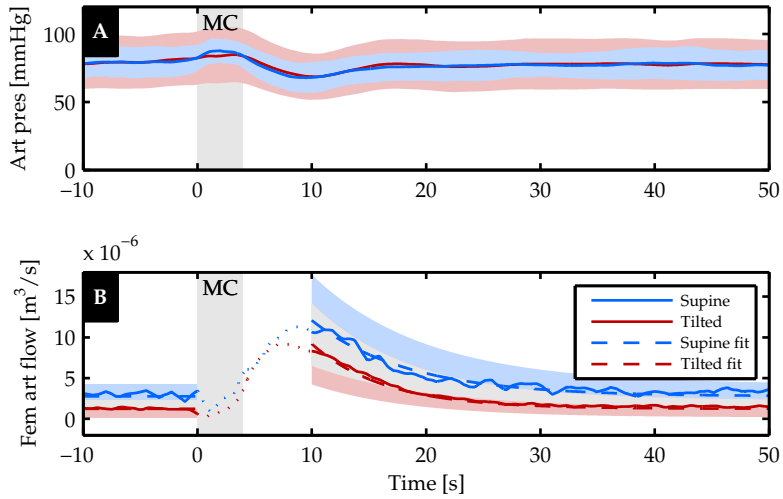

Figure 5: Heartbeat average of **A** the finger pressure and **B** femoral artery flow response to a muscle contraction in supine (red) and head up tilt (blue) position. The gray area indicates the 4-s muscle contraction (MC). Furthermore, the fit ($--$) to the flow response is included, where its uncertainty is indicated with the shaded area around (light gray indicates the overlap). The dotted line ($\cdot\cdot$; $0 < t < 10\ s$) indicates the uncertain part of the flow curve due to measurement difficulties. Fitting parameters and their standard deviation can be found in Table 3.

Table 3: Fitting parameters of the flow decay after muscle contraction using the following equation: $q_{\text{fit}}(t) = q_0 + (q_{\text{max}} - q_0)e^{-(t-t_{\text{max}})/\tau}$

	q_0 [mL/s]	q_{max} [mL/s]	τ [s]
Supine	2.8 ± 1.5	12.1 ± 5.6	8.4 ± 1.6
Head up tilt	1.2 ± 1.1	9.2 ± 5.0	6.4 ± 2.2

where $\overline{x}_{i_{\text{subj}}}(t)$ is the mean response of subject i_{subj}. The resulting time averaged pressure and femoral artery flow are shown in Figure 5A and B respectively, with the supine measurement in red and the head up tilt in blue. The area around the fitted curve represents one standard deviation from the average fit.

2.3 Simulations and analysis

The first aim is to match the simulated flow response during a supine muscle contraction to the fit of the measured data (Figure 5B), to gain insight into the importance of the various regulation mechanisms. An explorative local analysis including variation of x_{init}, $T_{\text{max},0}$, G_{meta} and G_{myo}, identified G_{meta} and G_{myo} as the major determinants. Therefore, G_{meta} and G_{myo} were varied ($-25 < G_{\text{meta}} < -15$; $dG_{\text{meta}} = 1$ and $0.5 < G_{\text{myo}} < 1.5$; $dG_{\text{myo}} = 0.25$) during the fitting procedure, while keeping all other regulation parameters at their baseline values (55 model evaluations). The best three sets of gains are derived based on the least square of the difference between the simulated flow response and the *in vivo* fit.

$$\epsilon = \int_{t=10\ s}^{50\ s} \sqrt{(q_{\text{sim}} - q_{\text{fit}})^2}\, dt. \tag{21}$$

These parameters are then used to repeat the simulation in the head up tilt position. Apart from obtaining a nice fit, the second aim of the first analysis is to determine the relative importance of the regulation mechanisms. Because the regulation mechanisms are included individually their relative importance can be analyzed directly.

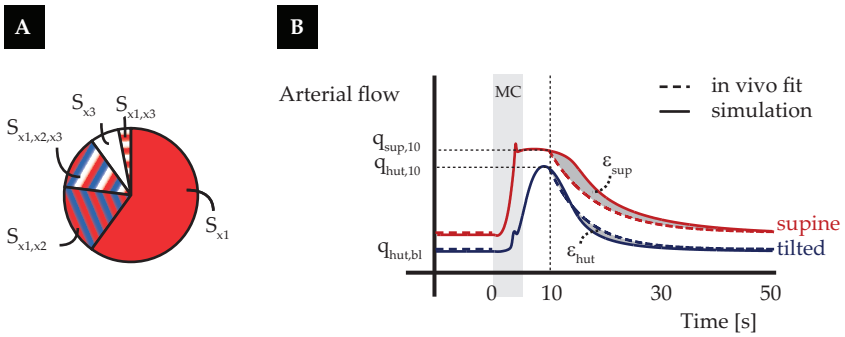

Figure 6: Sensitivity analysis **A** Schematic visualisation of the distribution of the output variance over the various input parameter and their interactions. S_i = main sensitivity index, S_{ij} = second order effect, S_{ijk} = third order effect. **B** Output of interest visualized in a plot of the flow response to a muscle contraction in supine and tilted position.

In the above mentioned analysis a constant pressure is used as an input for the baroreflex and the inlet boundary condition. However, *in vivo* the systemic pressure shows a small increase during and a decrease after muscle contraction (Figure 5). In a second analysis the influence of this pressure fluctuation via the systemic pressure and the baroreflex regulation on the flow response was investigated. For this the best parameter set, derived in the first analysis, was used to repeat the supine and tilted simulations with the following adaptations: (1) *in vivo* pressure is used as an input for the baroreflex and p_{inlet} remains unchanged compared to the previous simulations; (2) *in vivo* pressure is used as an input for the baroreflex as well as for p_{inlet}.

2.4 Sensitivity analysis

To investigate the importance of all regulation parameters on the flow response to a muscle contraction and to validate the choice to derive the fit based on only G_{meta} and G_{myo} as described in the previous section, a global sensitivity analysis was performed. Simultaneous variation of the input parameters within their uncertainty range enables the derivation of the variance in the simulated flow response. Each fraction of this output variance can be allocated to individual parameters or interaction between two or more input parameters (Figure 6A). The influence of an individual input parameter is captured by the main sensitivity index S_i, which can be interpreted as the expected reduction in output variance if the true value would have been known. The contribution of interaction between two or more parameters is captured by the higher order effects ($S_{ij}, S_{ijk}, ...$) [Eck et al., 2016].

2.4.1 Output of interest

The following parameters, describing the flow response to a muscle contraction in both supine and tilted position, are used as outputs of interest:

- $q_{\text{sup,max}}$: Flow in supine position $10\ s$ after the onset of muscle contraction.
- $\epsilon_{\text{sup}} = \int_{t=10\ s}^{50\ s} \sqrt{(q_{\text{sim,sup}} - q_{\text{fit,sup}})^2}$: Root mean square of the difference between the simulation and the fit of the flow response to a muscle contraction in the supine position.
- $q_{\text{hut,bl}}$: Baseline flow in the tilted position.
- $q_{\text{hut,max}}$: Flow in the tilted position $10\ s$ after the onset of muscle contraction.

- $\epsilon_{\text{hut}} = \int_{t=10\ s}^{50\ s} \sqrt{(q_{\text{sim,hut}} - q_{\text{fit,hut}})^2}$: Root mean square of the difference between the simulation and the fit of the flow response to a muscle contraction in the tilted position.

2.4.2 Input parameters

The sensitivity analysis was performed while varying all input parameters of the regulation model. A description of these parameters can be found in Table 4, along with their baseline value and the range used for the sensitivity analysis. The uncertainty ranges are based on literature values or values resulting in a physiological flow response determined by a local sensitivity analysis (results not shown). From this local sensitivity analysis, it was concluded thatr_m (the radius at which maximal tension can be reached) and r_t (the constant defining the shape of the maximal tension curve) should be fixed, as even small variation resulted in non-physiological responses or decreased model stability.

Table 4: Model input parameters included in the sensitivity analysis. Uncertainty range is given in percentages, unless indicated with superscript ABS when the absolute range is given. The uncertainty range is based on literature values and is adapted when the local sensitivity analysis indicated unphysiological outputs or decreasing in model stability.

Symbol	Value	Unit	Description	Range
$\sigma_{\text{e,0}}$	1.49	kPa	Parameter for elastic tension model (Laplace) [Ursino and Giammarco, 1991]	-10,7.5
K_σ	4.5	-	Parameter in tension model (Laplace) [Ursino and Giammarco, 1991]	-10,10
$r_{\text{a,0}}$	75.0	μ m	Arteriolar radius in unstressed condition (Laplace) [Ursino and Giammarco, 1991]	-10,10
σ_c	5.51	kPa	Stress contribution of collagen fibers (Laplace) [Ursino and Giammarco, 1991]	-10,10
$rh_{\text{a,0}}$	0.33	-	Unstressed arteriolar wall thickness relative to radius (Laplace) [Nordborg et al., 1985]	-10,10
η_a	6.37	kPa s	Arteriolar wall viscosity (Laplace) [Ursino and Giammarco, 1991]	-10,10
n_m	1.75	-	Parameter for smooth muscle tension model (Laplace) [Ursino and Giammarco, 1991, Ursino and Lodi, 1998]	-10,7.5
$T_{\text{max,0}}$	5.0	Pa	Smooth muscle tension in basal condition (Laplace) [Ursino and Giammarco, 1991, Ursino and Lodi, 1998]	4.0,5.5$^{\text{ABS}}$
x_{init}	-0.5	-	Offset regulation state (Laplace)	-0.6,-0.45$^{\text{ABS}}$
p_n	13.3	kPa	Reference pressure baroreflex model (Baroreflex) [Boron and Boulpaep, 2003]	-10,10
$f_{\text{ab,min}}$	2.52	s^{-1}	Minimal afferent firing rate (Baroreflex) [Ursino, 1998, Ursino and Magosso, 2000, van der Hout-van der Jagt et al., 2013]	-30,30
$f_{\text{ab,max}}$	47.78	s^{-1}	Maximal afferent firing rate (Baroreflex) [Ursino, 1998, Ursino and Magosso, 2000, van der Hout-van der Jagt et al., 2013]	-30,20

Table 4 – continued from previous page

Symbol	Value	Unit	Description	Range
k_{dp}	1.5676	kPa	Parameter defining slope of afferent firing rate (Baroreflex) [Ursino, 1998, Ursino and Magosso, 2000]	-20,30
$f_{\text{sp},\infty}$	2.1	s^{-1}	Sympathetic firing rate at infinite afferent firing rate (Baroreflex) [Ursino, 1998, Ursino and Magosso, 2000, van der Hout-van der Jagt et al., 2013]	-30,30
$f_{\text{sp},0}$	16.11	s^{-1}	Sympathetic firing rate at zero afferent firing rate (Baroreflex) [Ursino, 1998, Ursino and Magosso, 2000, van der Hout-van der Jagt et al., 2013]	-30,30
k_{es}	0.0675	s	Parameter defining the shape of the sympathetic firing rate (Baroreflex) [Ursino, 1998, Ursino and Magosso, 2000, van der Hout-van der Jagt et al., 2013]	-30,20
$f_{\text{sp,max}}$	60	s^{-1}	Maximal sympathetic firing rate (Baroreflex) [Ursino and Magosso, 2000, van der Hout-van der Jagt et al., 2013]	-30,30
G_R	0.33	MPa s m^{-3}	Gain baroreflex (Baroreflex) [Ursino and Magosso, 2000]	-30,15
D_R	2.0	s	Pure time delay sympathetic firing rate (Baroreflex) [Ursino, 1998, Ursino and Magosso, 2000, van der Hout-van der Jagt et al., 2013]	-30,30
$f_{\text{es,min}}$	2.66	s^{-1}	Minimal sympathetic firing rate affecting resistance (Baroreflex) [Ursino, 1998, Ursino and Magosso, 2000]	-30,20
τ_R	6.0	s	Time constant low pass filter baroreflex (Baroreflex) [Ursino, 1998, Ursino and Magosso, 2000, van der Hout-van der Jagt et al., 2013]	-30,30
V	300	mL	Volume estimation of perfused muscle tissue (Metabolic) [Elliott et al., 1997]	-10,10
$C_{\text{a,CO}_2}$	20.65	mol m^{-3}	Arterial CO_2 concentration (Metabolic)	$20.0,20.9^{\text{ABS}}$
f_m	75	-	Ratio of metabolism in rest and under maximal activity (Metabolic) [Boron and Boulpaep, 2003]	$75,85^{\text{ABS}}$
$A_{\text{mc,max}}$	0.3	–	Percentage of maximum EMG reached during muscle contraction (Metabolic) [Tschakovsky et al., 2004]	-30,15
ρ_m	1055	kg m^{-3}	Muscle density (Metabolic) [Segal et al., 1986]	$1040,1070^{\text{ABS}}$
$M_{\text{CO}_2,0,\text{m}}$	12.9	μmol s^{-1} kg^{-1}	Basal metabolic CO_2 production per kg muscle tissue (Metabolic) [Boron and Boulpaep, 2003]	$9.0,13.5^{\text{ABS}}$
$\alpha_{\text{t,v}}$	0.49	-	Fitting constant venous CO_2 concentration (Metabolic) [Irving et al., 1932]	$0.43,0.55^{\text{ABS}}$

Table 4 – continued from previous page

Symbol	Value	Unit	Description	Range
$\beta_{\text{t,v}}$	11.5	mol m^{-3}	Fitting constant venous CO_2 concentration (Metabolic) [Irving et al., 1932]	9.7,13.3$^{\text{ABS}}$
$C_{\text{v,CO}_2,0}$	22.34	mol m^{-3}	Venous CO_2 concentration at rest (Metabolic) [Geers and Gros, 2000]	22.1,23.0$^{\text{ABS}}$
G_{meta}	-15	-	Gain for metabolic mechanism (Metabolic)	-25,-10$^{\text{ABS}}$
τ_{meta}	15.0	s	Time-constant metabolic regulation (Metabolic) [Ursino and Lodi, 1998]	12,18$^{\text{ABS}}$
G_{myo}	0.75	-	Gain for myogenic mechanism (Myogenic)	0.1,5$^{\text{ABS}}$
τ_{meta}	7.0	s	Time-constant myogenic regulation (Myogenic) [Ursino and Lodi, 1998]	4,9$^{\text{ABS}}$

2.4.3 Morris screening and general polynomial chaos expansion

To derive the output variance and the sensitivity indices in a computationally efficient manner, the two-step approach described by Donders et al. [2015] was used. In the first step non-important model parameters are identified by using a Morris screening. In the second step the generalized polynomial chaos expansion method is applied to the reduced input space, resulting in a metamodel from which the sensitivity indices can be calculated straightforwardly [Huberts et al., 2014]. The metamodel consists of orthogonal polynomials dependent on the model parameters and with output-specific coefficients, which are derived by a least-square regression of the metamodel and N simulations. The accuracy of the metamodel is determined by the quality of the regression, for which a sufficient number of model evaluations is needed. In the current study a metamodel containing orthogonal polynomials up to the third order is derived based on 13485 model evaluations ($CPU \approx 63\ h$, using 25 cores). The number of model evaluations is based on: $N = \binom{z+k}{z} \cdot q$, where $z = 3$ is the order of the metamodel, $k = 28$ is the number of input parameters of the reduced input space and q is set to 3 to have sufficient simulations to obtain a good regression.

2.4.4 Post sensitivity analysis

To investigate how well the important parameters identified in the sensitivity analysis can fit the *in vivo* response two additional sets of simulations were performed. First, all parameters with $S_T > 0.05$ for at least one output of interest were varied randomly over $k * 500$ simulations, with k the number of parameters. Second, the same process was carried out for all parameters with $S_T > 0.10$. For both sets of simulations it was investigated which simulations were in good agreement with the *in vivo* fit, i.e. within the standard deviation of the *in vivo* fit. A second subset is defined to include all simulation within half the standard deviation. Finally, it is analysed how the input parameters of these subsets of simulations were distributed over the input space.

3 Results

This section first reports how the activation of the regulation mechanisms influences the agreement between the flow response and the *in vivo* data. Secondly, the influence of systemic pressure on the regulation is reported. Finally, the results of the sensitivity analysis are presented.

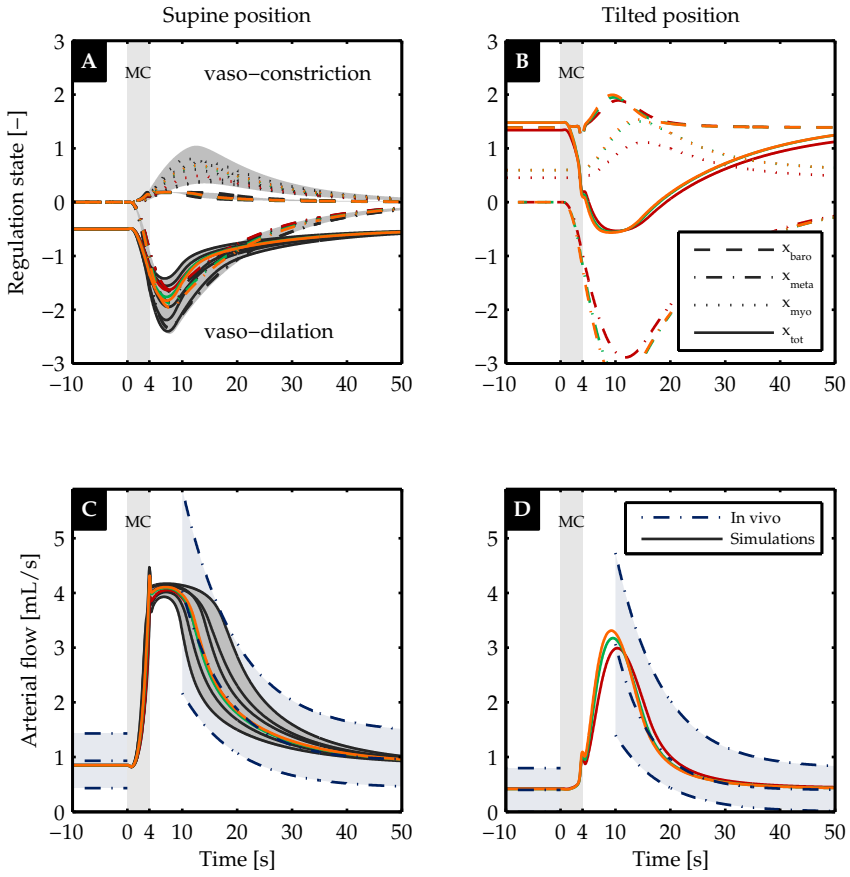

Figure 7: Regulatory response to muscle contraction in supine and tilted position, depicted in the left and right column respectively. In plot **A** and **B** the regulation state of the various mechanisms is shown over time: baroreflex (−−), metabolic (−·), myogenic (··) regulation and the sum of the three (−). Here, the negative state corresponds to vasodilation and the positive state to vasoconstriction. The resulting arterial flow is shown in plot **C** and **D** together with the fit to the *in vivo* response (−·). The three simulations best matching the *in vivo* response are depicted in color. The remaining simulations (as described in Section 2.3) are visualized together in the gray area. To show the general patterns some individual responses are depicted in dark gray.

3.1 Baseline simulations

The regulatory response to a muscle contraction in the supine position was simulated while varying the gain of the myogenic and metabolic mechanism. The variation in regulatory responses and arterial flow are indicated by the gray region either side of the curve in Figure 7A and C respectively. The period of muscle contraction (MC) is indicated by the shaded region ($0 < t < 4$ s). The arterial flow responses which best match the *in vivo* measurement (−· plus the standard deviation indicated by the blue area) are visualised in color. These parameters values are used to repeat the simulation in the tilted position, for which the results are shown in Figure 7B and D. For the best flow results the regulatory state of the baroreflex (−−), metabolic (−·) and myogenic (··) mechanism are also shown in color.

Before the onset of muscle contraction in the supine position all the regulation states are equal to zero. After muscle contraction ($t > 4$ s), the metabolic mechanism induces a strong vasodilation, whereas the myogenic mechanism and baroreflex show a mild and small vasoconstriction respectively (Figure 7A). Arterial flow shows an increase due to

the muscle contraction and a gradual decay starting at $t \approx 10\ s$, which closely matches the *in vivo* response (Figure 7C). Most of the remaining flow responses show waveforms that are parallel to each other, although some simulations cross due to a difference in decay (Figure 7C).
In the tilted position, the baroreflex and to a lesser extent the myogenic mechanisms induce a vasoconstriction at baseline ($-10 < t < 0\ s$). After muscle contraction ($t > 4\ s$), the metabolic response induces a vasodilation, slightly inhibited by the vasoconstrictive response of the myogenic mechanism and baroreflex (Figure 7B). Finally, arterial flow increases after muscle contraction and decreases back to baseline, matching the *in vivo* response (Figure 7D).

3.2 Influence of systemic pressure

The influence of the fluctuation in systemic pressure on the flow response to a muscle contraction is investigated. For this, the best fit found in the previous section is compared to a simulation with the pressure fluctuations included only in terms of the baroreflex regulation and a simulation with the pressure fluctuation applied at the inlet as well as the baroreflex. The regulatory (top) and flow (bottom) response to a muscle contraction in the supine (left) and tilted (right) position are shown in Figure 8.
In the supine position the three simulations all start at the same baseline and show a similar decay for $t > 10\ s$ (Figure 8C). Peak flow ($5 < t < 10\ s$) is lower once the pressure fluctuation is applied via baroreflex regulation (green line). In the case where the pressure fluctuation is also applied as an inlet boundary condition (orange line) a fast decrease is observed shortly after muscle contraction followed by a plateau. In the tilted position all three simulations start at the same baseline (Figure 8D). The flow decay for $t > 10\ s$ is faster for both simulations with the *in vivo* pressure applied compared to the original simulation, but remain close to the fit of the *in vivo* response (dashed dark blue line). Furthermore, peak flow is higher and is reached sooner following muscle contraction if the *in vivo* pressure is used.

3.3 Sensitivity analysis

3.3.1 Morris screening

From the Morris screening the following parameters were found to be unimportant: parameter for smooth muscle tension model n_{m}, minimal afferent firing rate (baroreflex) $f_{\mathrm{ab,min}}$, parameter defining shape of sympathetic firing rate (baroreflex) k_{es}, pure time delay of sympathetic firing rate (baroreflex) D_{R}, percentage of maximum EMG $A_{\mathrm{muscle,max}}$ and basal metabolic CO_2-production $M_{\mathrm{CO_2,0,m}}$. Excluding these six parameters from the polynomial chaos expansion reduces the required number of simulations from 23310 to 13485.

3.3.2 Polynomial chaos expansion

The quality of the derived metamodels, captured by the descriptive error, is shown in Table 5. This gives the part of the variance that could not be captured by the metamodel. For the ϵ_{sup} and ϵ_{hut} the descriptive error is relatively large; 0.14 and 0.10 respectively.
The total sensitivity indices for all outputs of interest are shown in Table 6. The input parameters are arranged in order of importance and only contributions greater than 1% are shown. The myogenic gain G_{myo} is the most important parameter for all outputs of interest. Furthermore, the metabolic gain G_{meta}, the initial regulation state x_{init} and the

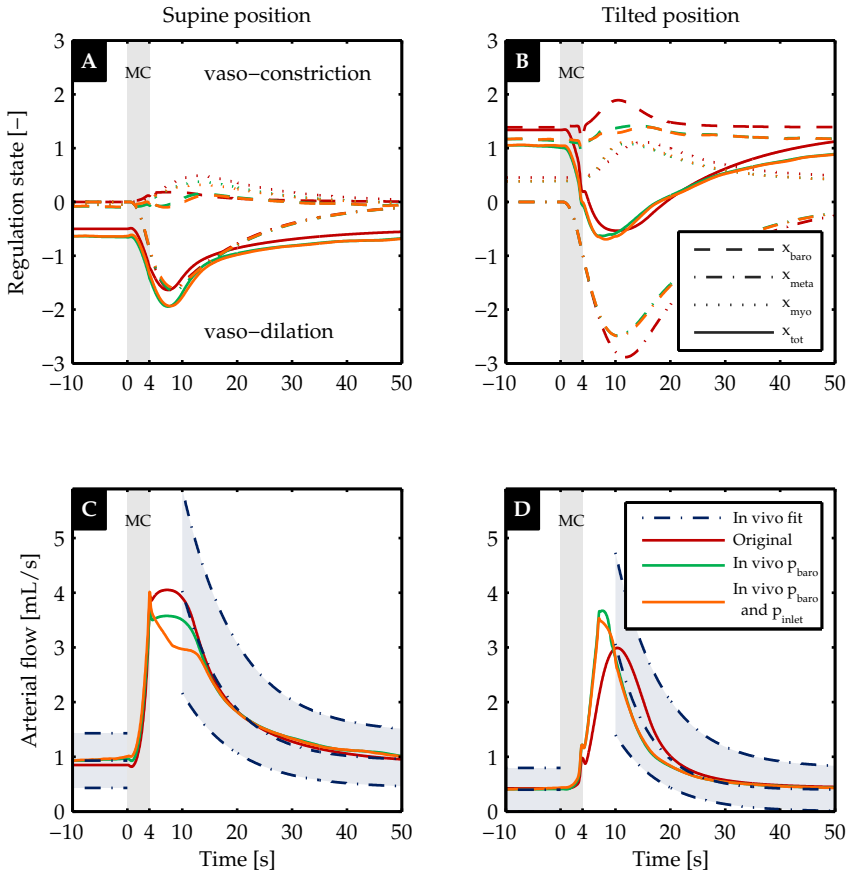

Figure 8: Influence of variation in systemic pressure on the regulatory response to muscle contraction in supine and tilted position (left and right column respectively). In plot **A** and **B** the regulation state of the various mechanisms is shown over time: baroreflex $(--)$, metabolic $(\cdot\cdot)$, myogenic $(-\cdot)$ regulation and the sum of the three $(-)$. Here, the negative state corresponds to vasodilation and the positive state to vasoconstriction. The resulting arterial flow is shown in plot **C** and **D** together with the fit to the *in vivo* response $(-\cdot)$. The various colors represent the original simulation (red line), *in vivo* pressure applied at the baroreflex (green line) and *in vivo* pressure applied to both the baroreflex and the inlet boundary condition (orange line).

Table 5: Quality of the metamodel for each output of interest: $q_{\text{max,sup}}$, ϵ_{sup}, $q_{\text{bl,hut}}$, $q_{\text{max,hut}}$ and ϵ_{hut}. The error measure $1 - R^2$ can be interpreted as the residual variance that could not be captured by the metamodel.

	$q_{\text{max,sup}}$	ϵ_{sup}	$q_{\text{bl,hut}}$	$q_{\text{max,hut}}$	ϵ_{hut}
$1 - R^2$	0.04	0.14	0.01	0.06	0.10

Table 6: Total sensitivity indices of all the outputs of interest: $q_{\text{max,sup}}$, ϵ_{sup}, $q_{\text{bl,hut}}$, $q_{\text{max,hut}}$ and ϵ_{hut}. The input parameters are arranged in order of importance and only contributions starting at 1% are shown.

	$q_{\text{max,sup}}$	ϵ_{sup}	$q_{\text{bl,hut}}$	$q_{\text{max,hut}}$	ϵ_{hut}
G_{myo}	0.79	0.72	0.55	0.64	0.47
G_{meta}	0.08	0.17		0.18	0.30
x_{init}		0.02	0.38	0.04	0.11
τ_{meta}		0.16		0.02	0.09
$C_{\text{v,CO}_2,0}$	0.02	0.06		0.05	0.09
$C_{\text{a,CO}_2}$	0.02	0.06		0.05	0.09
r_0	0.06	0.06	0.02	0.01	0.02
$T_{\text{max,0}}$	0.03	0.03	0.01	0.03	0.05
τ_{myo}		0.08			0.03
$f_{\text{ab,max}}$		0.01	0.02	0.02	0.05
f_{m}	0.02	0.05		0.01	0.02
G_{R}		0.02	0.02	0.02	0.04
p_{n}	0.01	0.02	0.04	0.01	0.02
k_{dp}		0.01	0.01	0.02	0.03
K_σ	0.03	0.03			
$f_{\text{es,min}}$		0.02		0.01	0.03
$f_{\text{sp},\infty}$		0.01		0.01	0.03
$f_{\text{sp,0}}$		0.02			0.01
σ_{e0}		0.02			
rh_0		0.02			
V		0.02			
α_{tv}		0.02			
σ_c		0.01			
η_a		0.01			
$f_{\text{sp,max}}$		0.01			
τ_{R}		0.01			
ρ_{m}		0.01			
β_{tv}		0.01			

metabolic time constant τ_{meta} all contribute more than 10% to the variance for at least one output of interest. This is in line with the first local analysis where a fit was derived based on G_{myo} and G_{meta}. Four other parameters have a contribution larger than 5%: $C_{\text{v,CO}_2,0}$, $C_{\text{a,CO}_2}$, r_0 and τ_{myo}. All other parameters have a smaller contribution, but they do all contribute to the variance of the output.

The main sensitivity indices and higher order interactions are shown in Figure 9, where the main sensitivity indices S_i are shown as ellipsoids, the second order interactions are indicated by an arrow and the third order interactions by a shaded area. The myogenic gain contributes most to the output variance; it has the highest main sensitivity index for all outputs of interest and is present in all of the main interactions. Furthermore, the metabolic gain G_{meta}, the initial regulation state x_{init} and the metabolic time constant τ_{meta} all have a main sensitivity index and/or interaction larger than 0.05 for at least one output of interest. The sums of the sensitivity indices (bottom of each subfigure) show that most of the variance is captured by individual contributions (S_i). However, for ϵ_{sup} and ϵ_{hut} a significant contribution to the variance comes from interactions between parameters. The contribution of the parameters varies for each regulation mechanism. The influence of the metabolic parameters is mainly observed in the maximum flow and ϵ outputs. The baroreflex parameters, on the other hand, are of more importance for the variance in baseline flow in the tilted position and the ϵ in tilted position. The parameters describing the myogenic mechanism and Laplace law are present in all outputs of interest.

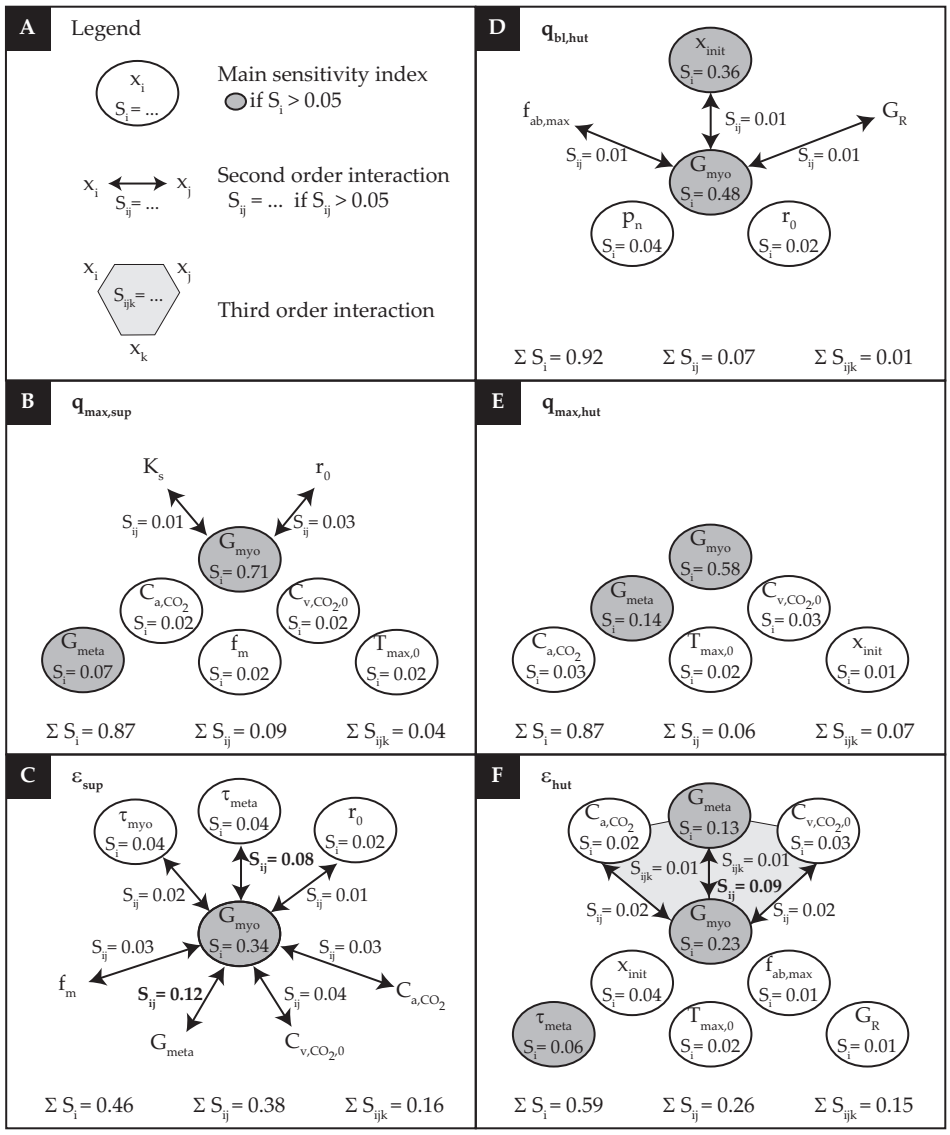

Figure 9: Results of the sensitivity analysis for all the outputs of interest: **B** $q_{\text{max,sup}}$, **C** $rmsq_{\text{sup}}$, **D** $q_{\text{bl,hut}}$, **E** $q_{\text{max,hut}}$ and **F** $rmsq_{\text{hut}}$. The main sensitivity index is visualised in a circle, the second order interaction with an arrow and the third order interaction with an area. For clarity only the contributions larger than 1% are shown. The most important parameters and interactions (with a contribution more than 5%) are highlighted with a gray background or bold font respectively. The sum of the main sensitivity indices, the sum of the second order interactions and the sum of the third order interactions are shown at the bottom of each subfigure.

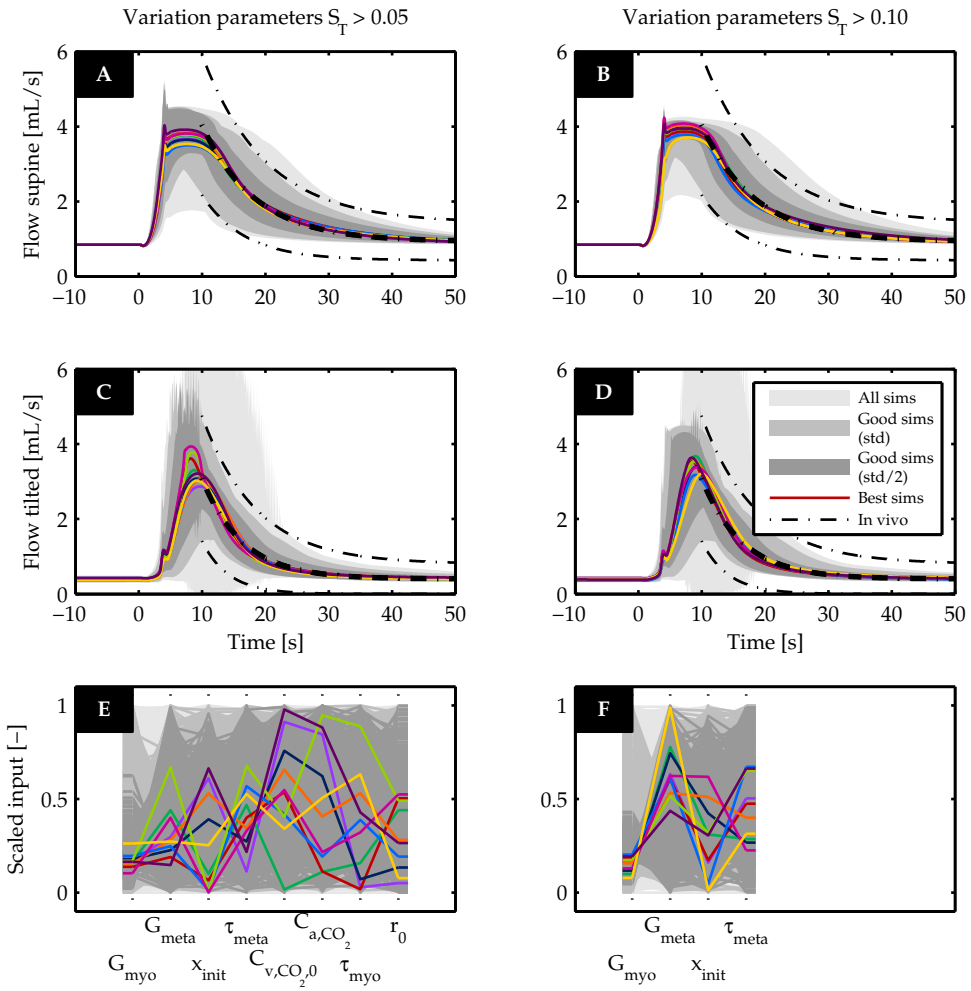

Figure 10: Post sensitivity analysis. The flow response of additional simulations varying the input parameters with $S_T > 0.05$ (left column) and $S_T > 0.10$ (right column) in both supine (**AB**) and tilted position (**CD**). For both sets the good simulations (present within one standard deviation and half the standard deviation) are presented in dark gray and the best 10 simulations in color. In the bottom plots (**EF**) the distribution of the corresponding input parameter is shown.

3.3.3 Post sensitivity analysis

The important parameters identified though the sensitivity analysis were used to perform two sets of simulations: (1) varying all parameters with $S_T > 0.05$ ($k = 8$) and (2) varying all parameters with $S_T > 0.10$ ($k = 4$). The flow response in both the supine and tilted positions together with the distribution of the input parameters is shown in Figure 10. Both sets of simulations are divided into four subsets: (1) the simulations that converged (light gray) (2) the simulations that had a flow response within the standard deviation of the *in vivo* fit (middle gray) (3) the simulation that had a flow response within half a standard deviation (dark gray) and (4) the 10 simulations which best matched the mean *in vivo* response (colors).
For the first set of 4000 simulations ($S_T > 0.05$) 1610 of the 3880 (41%) converged simulations had a flow response within one standard deviation of the *in vivo* response (mid gray in Figure 10AC). Taking only half the standard deviation into account only 385 (10%) simulations remained (dark gray). In Figure 10E it can be observed that all values of the input parameters can result in a flow response within the *in vivo* uncertainty, because the

light gray area covers the whole input space. However, some combinations never occur; e.g. G_{myo} and G_{meta} never have their maximum value simultaneously. When considering the simulations within half a standard deviation, a decrease in the input range of G_{myo} is observed (Figure 10E). The ten best simulations closely match the mean *in vivo* response in both positions (Figure 10AC). The distribution of the input parameters is more spread over the input domain once the importance of the parameter decreases (parameter importance decreases from left to right). Whereas the most important parameter G_{myo} has relative values between 0.10 and 0.27, values of the less important parameters, $C_{\text{v,CO}_2,0}$, $C_{\text{a,CO}_2,0}$ and τ_{myo}, cover the full input domain.
In the second set of 2000 simulations ($S_T > 0.10$) 1104 out of 1961 (56%) converged simulations showed a flow response within the *in vivo* uncertainty (mid gray in Figure 10BD). Considering only half a standard deviation results in only 277 (14%) simulations. Similar to the larger set of simulations, the input parameters of the good simulations (within one standard deviation) had values within their whole uncertainty range (mid gray Figure 10F). Again, not all combinations were present, especially at the lower and upper limits of the domains. For the subset within half a standard deviation a decrease in input range of G_{myo} is observed as for the first set of simulations. Although the value of ϵ_{sup} and ϵ_{hut} slightly increased (same order of magnitude), the 10 best simulations still closely matched the *in vivo* fit. However, now the values of G_{meta} show a stronger correlation with the values of G_{myo}, which is in line with the high values found in the sensitivity analysis for the interaction between G_{myo} and G_{meta}. Furthermore, the range of G_{meta} has shifted to the upper part of the domain, which indicates G_{meta} could be fixed within this range to obtain a good fit.

4 Discussion

The flow augmentation observed at the onset of exercise is hypothesized to be a result of the muscle pump effect, the regulation of vascular tone or a combination of both. In a previous study [Keijsers et al., 2015], we showed that the muscle pump effect alone cannot induce the flow increase observed *in vivo*. Therefore, in the current study the importance of the major mechanisms regulating blood flow during the different phases of a muscle contraction has been investigated in both the supine and tilted position. To investigate these effects our arterio-venous 1D pulse wave propagation model [Keijsers et al., 2015] has been extended with a regulation model accounting for baroreflex, metabolic and myogenic regulation. Model parameters were either taken from literature or determined by fitting the simulated arterial flow response to the measured *in vivo* response to a muscle contraction in the supine position. The model was then validated by comparing simulated results with the *in vivo* measurements in the tilted position without changing the parameter values obtained from the fit in the supine position. Furthermore, a sensitivity analysis has been performed to quantify the importance of the input parameters in the regulation model.
The model was able to capture the *in vivo* response in the supine position when only optimizing the values of the myogenic and metabolic gain (Figure 7C). When the same parameters were used to simulate a muscle contraction in the tilted position, again good agreement was found (Figure 7D). The model response replicates two of the main features of flow variation. Firstly, it matches the flow decay back to baseline after the vasodilation is initiated following muscle contraction. Secondly, the model captures the decreased baseline flow in the tilted position observed *in vivo*. Examining the activation of the various regulation mechanisms, the metabolic mechanism is the main vasodilator after muscle contraction in both the supine and tilted position, which is in line with *in vivo* studies [Nådland et al., 2009, Tschakovsky and Sheriff, 2004]. Furthermore, these simu-

lations support the hypothesis of Nådland et al. [2009] that the decrease in baseline flow in the tilted position is a result of the global baroreflex and local myogenic activation. The latter is a result of the decreased carotid pressure and increased arteriolar pressure respectively.
The influence of the variation in systemic pressure via the baroreflex mechanism and the boundary conditions of the model is assessed and is most clearly observed within the first $10\ s$ after the onset of muscle contraction (Figure 8). The lack of reliable *in vivo* data shortly after muscle contraction, does not allow any conclusions to be drawn on which implementation is closest to physiology. The relatively small effect during the remaining part of the response ($t > 10$s) can be explained by the fact that most of the variation in systemic pressure is present shortly after muscle contraction. In the *in vivo* study of Nådland et al. [2009] it was stated that the systemic pressure reduction was too small to have an effect on femoral artery flow. However, based on the combination of the current model results and *in vivo* measurements this statement can neither be confirmed nor rejected. Because the current study focusses on the flow decay after muscle contraction and the baseline flow, which are both hardly affected, the systemic pressure variation is not expected to have a large influence on the results.
Based on the sensitivity analysis, the spread in myogenic gain G_{myo} is clearly the most important parameter (both individually and through interactions) of the regulation model for variance in the simulated flow response to muscle contraction (Figure 9). The uncertainty in metabolic gain G_{meta} also has a significant contribution to the output variance. The importance of both gains was expected, because they determine the magnitude of vasodilation. Furthermore, it confirms the choice to vary G_{myo} and G_{meta} in the first analysis. The fact that G_{myo} is more important than G_{meta} may be a result of the sigmoid function (Equation (30)) that is applied to the total regulation state. Even a small myogenic activation (i.e. vasoconstriction) will shift the total regulation towards the more sensitive part of the regulation curve. A third important parameter is x_{init}, which is the offset of the regulation state. A change in x_{init} can shift the regulatory response to a less or more sensitive region of the regulation curve. This explains the large importance of x_{init} for $q_{\text{bl,hut}}$. The fourth important parameter is the metabolic time-constant τ_{meta}, which is expectedly important for both ϵ outputs. The fact that the metabolic parameters dominate the ϵ output is logical, because the metabolic activation was concluded to be the main vasodilator after muscle contraction. The baroreflex is almost inactive in the supine position, which is confirmed by the fact that the baroreflex parameters are not present for the supine outputs. Whilst the current model may seem complex, the large contribution of the higher order terms (S_{ij} and S_{ijk} in Figure 9) indicates the need of all parameter interactions in capturing the complex physiology of the system and thereby that the model is not too complex.
In the post sensitivity analysis it was concluded that even when only varying the 4 most important parameters (each contributing more than 10%), it was still possible to find simulations that strongly resemble the *in vivo* response. The small range found for G_{myo} for the 10 best fits confirms the importance of G_{myo}. Furthermore, the interaction between G_{myo} and G_{meta} was also confirmed, because high values of the two parameters never occur simultaneously. Examining the relation between G_{myo} and G_{meta} for the 10 best fits, even suggests defining a relation between the two. The large spread of input parameters observed for the subset of simulations within the measurement uncertainty, could indicate that the whole input space is not covered. However, analysing the simulations with a flow response within half a standard deviation indicates that if one could reduce the measurement uncertainty, the input space of the most important parameter G_{myo} could be decreased.
To model the regulation of vascular tone a general approach is taken using the mean ar-

teriolar radius as a measure for the regulatory state, because the explicit representation of individual arterioles was not of interest in the current study. Metabolic regulation was included based on a single metabolite, whereas many metabolites are known to act as vasodilator and no single metabolite has been shown to account for the full vasodilatory response [Joyner and Casey, 2015]. However, the current implementation is in good agreement with the *in vivo* response, which indicates that the tissue CO_2-concentration is a good surrogate for the general metabolic response. For a correct myogenic activation an accurate pressure level is necessary. As only the calf circulation is included in the 1D part, the hydrostatic column applied to the pressure boundary condition might be overestimated, especially on the venous side. This could be overcome if the proximal vasculature would also be included in the 1D part of the model. However, as the current model is able to accurately match the *in vivo* response, it is concluded that the current model contains sufficient detail to capture the flow response after muscle contraction.
For validation of the developed model, *in vivo* ultrasound measurements were performed capturing the flow response to a calf muscle contraction in both the supine and tilted positions (Figure 5B). Measured baseline flow in the supine position was observed to be 2.3 times higher than in the 70° head up tilt position (Table 3), which is in line with the flow decrease observed by Nådland et al. [2009] in the 30° head up tilt position. Flow changes observed following muscle contraction reach peak flow within $10\ s$ followed by a decay back to baseline within a further minute. This is in accordance with the changes observed by Tschakovsky et al. [1996] following a single forearm contraction and those observed by Wesche [1986] following quadriceps contraction. Although the general flow response is in accordance with previous *in vivo* studies, the first $10\ s$ after the onset of muscle contraction are excluded from the validation, because this part of the measurement is less accurate due to measurement difficulties during and shortly after muscle contraction. Improved measurements are necessary for validation of the simulated flow response in the first $10\ s$ after muscle contraction, which could possible be obtained by fixing the ultrasound probe to the subject.
The quality of the metamodel, captured in the coefficient of determination ($1 - R^2$), was observed to be lower for the outputs ϵ_{sup} and ϵ_{hut}. Because both outputs cover a time range of $40\ s$, they include more information, which is more likely to be hard to capture in a metamodel. Furthermore, these effects could be due to the fact that the importance of the parameters excluded by the Morris screening was underestimated. However, the post sensitivity analysis shows that even when varying only the four most important parameters the model is capable to capture the flow response to a muscle contraction. Another more likely reason is that the variance that could not be captured by the metamodel is a result of the high frequency vibrations present in some simulations, because the ϵ outputs are affected most by these instabilities. Further research is needed to improve model stability. However, the values of the coefficient of determination are still acceptable and are not expected to influence the results.
This study has described how the developed model can be used to study the regulation of vascular tone in healthy individuals under muscle contraction. However, this model has potential application in the study of chronic venous disease. Extending the current model with regurgitating valves [Mynard et al., 2012] or valve prolapse [Pant et al., 2015], would allow examination of valve dynamics and hemodynamics in the presence of disease. Furthermore, the model could be used to simulate the effect of multiple contractions, as studied by Simakov et al. [2013], or even exercise. For the latter application, an extension of the model to the full circulation [Müller and Toro, 2014, Mynard and Smolich, 2015] is needed to account for venous return and baroreflex regulation of heart rate and heart contractility. This would also improve the model with a better representation of the full hydrostatic column.

5 Conclusion

A 1D pulse wave propagation model was developed including the baroreflex, metabolic and myogenic regulation, which enables the simulation of the flow response to a muscle contraction. In addition to our previously presented model [Keijsers et al., 2015], which considered only the mechanical effect of a muscle contraction (muscle pump), we added a regulation model and now the simulated flow response accurately mimicks the *in vivo* measurements in both the supine and tilted positions. This confirms the hypothesis that regulation of peripheral resistance is an important mechanism inducing the flow increase at the onset of exercise. From the activation of the regulatory mechanisms it is concluded that (1) metabolic activation is the main vasodilator after muscle contraction and (2) baroreflex and myogenic activation are responsible for the decrease in baseline flow in the tilted position. The sensitivity analysis confirmed G_{myo} as the most important parameter.

Acknowledgements

J.M.T. Keijsers received a scholarship of the Helmholtz SpaceLife Sciences Research School (SpaceLife) which was funded by the Helmholtz Association and the German Aerospace Center (Deutsches Zentrum für Luft- und Raumfahrt e.V., DLR). The contribution of Dr. A.J. Narracott to this research was supported by funding from the Research Mobility Programme of the Worldwide Universities Network. The contribution of Dr. C.A.D Leguy was performed with the support of the Marie Curie International Outgoing fellowship of the European's 7th Framework Programme for Research under contract number MC-IOF-297967

References

References

D. Bessems, M. Rutten, and F. Van De Vosse. A wave propagation model of blood flow in large vessels using an approximate velocity profile function. *J Fluid Mech*, 580:145–168, 2007.

W. F. Boron and E. L. Boulpaep. *Medical Physiology: Updated Edition*. Elsevier Health Sciences, 2003.

W. P. Donders, W. Huberts, F. N. van de Vosse, and T. Delhaas. Personalization of models with many model parameters: an efficient sensitivity analysis approach. *Int J Numer Method Biomed Eng*, 31(10):e02727, 2015.

V. G. Eck, W. P. Donders, J. Sturdy, J. Feinberg, T. Delhaas, L. R. Hellevik, and W. Huberts. A guide to uncertainty quantification and sensitivity analysis for cardiovascular applications. *Int J Numer Method Biomed Eng*, 32(8):e02755, 2016.

M. A. Elliott, G. A. Walter, H. Gulish, A. S. Sadi, D. D. Lawson, W. Jaffe, E. K. Insko, J. S. Leigh, and K. Vandenborne. Volumetric measurement of human calf muscle from magnetic resonance imaging. *MAGMA*, 5(2):93–98, 1997.

Y. Fung. *Biomechanics: mechanical properties of living tissues*. Springer New York, 1993.

C. Geers and G. Gros. Carbon dioxide transport and carbonic anhydrase in blood and muscle. *Physiol Rev*, 80(2):681–715, 2000.

S. D. Gray, C. Staub, D. Sarah, E. Carlsson, and N. C. Staub. Site of increased vascular resistance during isometric muscle contraction. *Am J Physiol*, 213(3):683–689, 1967.

W. Huberts, W. P. Donders, T. Delhaas, and F. N. van de Vosse. Applicability of the polynomial chaos expansion method for personalization of a cardiovascular pulse wave propagation model. *Int J Numer Method Biomed Eng*, 30:1679–1704, 2014.

L. Irving, H. C. Foster, and J. K. W. Ferguson. The carbon dioxide dissociation curve of living mammalian muscle. *J Biol Chem*, 95(1):95–113, 1932.

M. J. Joyner and D. P. Casey. Regulation of increased blood flow (hyperemia) to muscles during exercise: a hierarchy of competing physiological needs. *Physiol Rev*, 95:549–601, 2015.

J. M. T. Keijsers, C. A. D. Leguy, W. Huberts, A. J. Narracott, J. Rittweger, and F. N. van de Vosse. A 1D pulse wave propagation model of the hemodynamics of calf muscle pump function. *Int J Numer Method Biomed Eng*, 31(7):e02714, 2015.

J. M. T. Keijsers, C. A. D. Leguy, W. Huberts, A. J. Narracott, J. Rittweger, and F. N. van de Vosse. Global sensitivity analysis of a model for venous valve dynamics. *J Biomech*, 49 (13):2845–2853, 2016.

T. Kenner. The measurement of blood density and its meaning. *Basic Res Cardiol*, 84(2): 111–124, 1989.

W. Kroon, W. Huberts, M. Bosboom, and F. van de Vosse. A numerical method of reduced complexity for simulating vascular hemodynamics using coupled 0D lumped and 1D wave propagation models. *Comput Math Methods Med*, 2012:156094, 2012.

C. A. D. Leguy, E. M. H. Bosboom, A. P. G. Hoeks, and F. N. van de Vosse. Model-based assessment of dynamic arterial blood volume flow from ultrasound measurements. *Med Biol Eng Comput*, 47:641–648, 2009.

R. L. Letcher, S. Chien, T. G. Pickering, J. E. Sealey, and J. H. Laragh. Direct relationship between blood pressure and blood viscosity in normal and hypertensive subjects: role of fibrinogen and concentration. *Am J Med*, 70(6):1195–1202, 1981.

E. Lim, G. S. H. Chan, So. Dokos, S. C. Ng, L. A. Latif, S. Vandenberghe, M. Karunanithi, and N. H. Lovell. A Cardiovascular Mathematical Model of Graded Head- Up Tilt. *PLoS One*, 8(10):e77357, 2013.

M. H. Meissner. Lower extremity venous anatomy. *Semin Intervent Radiol*, 22(3):147–156, 2005.

L. O. Müller and E. F. Toro. A global multiscale mathematical model for the human circulation with emphasis on the venous system. *Int J Numer Method Biomed Eng*, 30(7): 681–725, 2014.

J. P. Mynard and J. J. Smolich. One-Dimensional Haemodynamic Modeling and Wave Dynamics in the Entire Adult Circulation. *Ann Biomed Eng*, 43(6):1443–1460, 2015.

J. P. Mynard, M. R. Davidson, D. J. Penny, and J. J. Smolich. A simple, versatile valve model for use in lumped parameter and one-dimensional cardiovascular models. *Int J Numer Method Biomed Eng*, 28:626–641, 2012.

I. H. Nådland, L. Walløe, and K. Toska. Effect of the leg muscle pump on the rise in muscle perfusion during muscle work in humans. *Eur J Appl Physiol*, 105(6):829–841, 2009.

C. Nordborg, K. Fredriksson, and B. B. Johansson. The Morphometry of Consecutive Segments in Cerebral Arteries of Normotensive and Spontaneously Hypertensive Rats. *Stroke*, 16(2):313–320, 1985.

M. S. Olufsen, H. T. Tran, J. T. Ottesen, Research Experiences for Undergraduates Program, L. A. Lipsitz, and V. Novak. Modeling baroreflex regulation of heart rate during orthostatic stress. *Am J Physiol Regul Integr Comp Physiol*, 291:R1355–R1368, 2006.

S. Pant, C. Corsini, C. Baker, T. Y. Hsia, G. Pennati, and I. E. Vignon-Clementel. Data assimilation and modelling of patient-specific single-ventricle physiology with and without valve regurgitation. *J Biomech*, pages 1–12, 2015.

L. B. Rowell. *Human Cardiovascular Control*. Oxford University Press, 1993.

S. S. Segal, T. P. White, and J. A. Faulkner. Architecture, composition, and contractile properties of rat soleus muscle grafts. *Am J Physiol*, 250(19):C474–C479, 1986.

A. H. Shapiro. Steady flow in collapsible tubes. *J Biomech Eng*, 99(3):126–147, 1977.

S. Simakov, T. Gamilov, and Y. N. Soe. Computational study of blood flow in lower extremities under intense physical load. *Russ J Numer Anal M*, 28(5):485–503, 2013.

B. Spronck, E. G. H. J. Martens, E. D. Gommer, and F. N. van de Vosse. A lumped parameter model of cerebral blood flow control combining cerebral autoregulation and neurovascular coupling. *Am J Physiol Heart Circ Physiol*, 303:H1143–H1153, 2012.

M. E. Tschakovsky and D. D. Sheriff. Immediate exercise hyperemia: contributions of the muscle pump vs. rapid vasodilation. *J Appl Physiol*, 97(2):739–747, 2004.

M. E. Tschakovsky, J. K. Shoemaker, and R. L. Hughson. Vasodilation and muscle pump contribution to immediate exercise hyperemia. *Am J Physiol*, 271(4):H1697–H1701, 1996.

M. E. Tschakovsky, A. M. Rogers, K. E. Pyke, N. R. Saunders, N. Glenn, S. J. Lee, T. Weissgerber, and E. M. Dwyer. Immediate exercise hyperemia in humans is contraction intensity dependent: evidence for rapid vasodilation. *J Appl Physiol*, 96(2):639–644, 2004.

M. Ursino. A mathematical study of human intracranial hydrodynamics part 1 - the cerebrospinal fluid pulse pressure. *Ann Biomed Eng*, 16(4):379–401, 1988.

M. Ursino. Interaction between carotid baroregulation and the pulsating heart: a mathematical model. *Am J Physiol*, 275(44):H1733–H1747, 1998.

M. Ursino and P. D. Giammarco. A Mathematical Model of the Relationship Between Cerebral Blood Volume and Intracraniai Pressure Changes: The Generation of Plateau Waves. *Ann Biomed Eng*, 19(1):15–42, 1991.

M. Ursino and C. A. Lodi. Interaction among auto-regulation, CO2 reactivity, and intracranial pressure: a mathematical model. *Am J Physiol*, 274(43):H1715–H1728, 1998.

M. Ursino and E. Magosso. Acute cardiovascular response to isocapnic hypoxia. I. A mathematical model. *Am J Physiol Heart Circ Physiol*, 279:H149–H165, 2000.

M. Ursino and E. Magosso. Role of short-term cardiovascular regulation in heart period variability: a modeling study. *Am J Physiol Heart Circ Physiol*, 284:H1479–H1493, 2003.

M. B. van der Hout-van der Jagt, S. G. Oei, and P. H. M. Bovendeerd. Simulation of reflex late decelerations in labor with a mathematical model. *Early Hum Dev*, 89:7–19, 2013.

J. Wesche. The time course and magnitude of blood flow changes in the human quadriceps muscles following isometric contraction. *J Physiol*, 377:445–462, 1986.

N. Westerhof, F. Bosman, C. J. de Vries, and A. Noordergraaf. Analog studies of the human systemic arterial tree. *J Biomech*, 2:121–143, 1969.

A Extravascular pressure

The temporal course of the extra vascular pressure is defined by

$$k(t) = \begin{cases} 0 & \text{if} \quad t < T_0 \\ \frac{1}{2}\left(1 + \sin(\frac{\pi(t-T_0)}{T_r} - \frac{\pi}{2})\right) & \text{if} \quad T_0 < t < T_0 + T_r \\ 1 & \text{if} \quad T_0 + T_r < t < T_0 + T_r + T_c \\ \frac{1}{2}\left(1 + \sin(\frac{\pi(t-T_0-T_r-T_c)}{T_f} + \frac{\pi}{2})\right) & \text{if} \quad T_0 + T_r + T_c < t < T_0 + T_r + T_c + T_f \\ 0 & \text{if} \quad t > T_0 + T_r + T_c + T_f \end{cases} \tag{22}$$

where $T_0 = 0\ s$ is the starting time of the compression, $T_r = 1\ s$ and $T_f = 1\ s$ are the times for the extravascular pressure to rise and fall respectively and $T_c = 2\ s$ is the time for the extravascular pressure to remain constant. The spatial course of the extravascular pressure is defined by

$$m(z) = \begin{cases} 0 & \text{if} \quad z < l_0 \\ \frac{1}{2}\left(1 + \sin(\frac{\pi(z-l_0)}{l_r} - \frac{\pi}{2})\right) & \text{if} \quad l_0 < z < l_0 + l_r \\ 1 & \text{if} \quad l_0 + l_r < z < l_{\text{end}} - l_f \\ \frac{1}{2}\left(1 + \sin(\frac{\pi(z-l_{\text{end}})}{l_f} + \frac{\pi}{2})\right) & \text{if} \quad l_{\text{end}} - l_f < z < l_{\text{end}} \\ 0 & \text{if} \quad z > l_{\text{end}} \end{cases} \tag{23}$$

where $l_0 = 0.07\ m$ and $l_{\text{end}} = 0.27\ m$ are the coordinates below and above which no extravascular pressure is applied and $l_r = 0.10\ m$ and $l_f = 0.10\ m$ are the lengths over which the extravascular pressure rises and falls. The z-coordinate is defined to be zero at the distal side of the vein and increases to $z = 0.34\ m$ at the proximal side.

B Regulation model

The regulation of vascular tone is based on three regulation mechanisms: myogenic regulation, metabolic regulation and the baroreflex. The activation of the different mechanisms and how they result in a change in resistance and compliance is explained in detail in the following sections.

B.1 Laplace's law

The arteriolar wall tension T_{tot} is the parameter determining vascular tone and is related to the arteriolar radius r_a via the Laplace law [Fung, 1993].

$$T_{\text{tot}} = p_a r_a - p_{ex}(r_a + h_a), \tag{24}$$

where p_a is the arteriolar pressure and h_a is the arteriolar wall thickness. The total tension is divided into three components: $T_{\text{tot}} = T_e + T_v + T_m$, where T_e, T_v and T_m are

the elastic, viscous and active smooth muscle tension respectively. The passive elastic tension is based on experimental studies and is defined by the exponential function [Ursino and Giammarco, 1991]

$$T_e = h_a \sigma_e = h_a \left(\sigma_{e,0} \left(e^{K_\sigma \cdot \frac{r_a - r_{a,0}}{r_{a,0}}} - 1 \right) - \sigma_c \right), \tag{25}$$

where $\sigma_{e,0}$ and K_σ are parameters defining the shape of the function, $r_{a,0}$ is the vessel radius in the unstressed condition and σ_c is the stress contribution of the collagen fibers. Furthermore, the arteriolar wall thickness h_a is defined by assuming no longitudinal stretch and conservation of mass:

$$h_a = \sqrt{r_a^2 + 2 r_{a,0} h_{a,0} + h_{a,0}^2} - r_a, \tag{26}$$

where $h_{a,0}$ is the unstressed arteriolar wall thickness.
The second component of the passive tension is the viscous tension T_v, which is in accordance with the viscous component of the Voigt model [Ursino and Giammarco, 1991]

$$T_v = \sigma_v h_a = \frac{\eta_a}{r_{a,0}} \frac{dr_a}{dt} h_a, \tag{27}$$

where η_a is the arteriolar wall viscosity.
The active smooth muscle tension T_m is known to decrease for very small and very large arteriolar radius and is therefore based on the following bell-type curve [Ursino and Giammarco, 1991]

$$T_m = T_{\text{max}} \cdot e^{-\left| \frac{r_a - r_m}{r_t - r_m} \right|^{n_m}}, \tag{28}$$

where r_m is the radius at which the smooth muscle cell exerts maximal tension, and r_t and n_m are constants. Furthermore, the maximal active tension T_{max} is defined by

$$T_{\text{max}} = T_{\text{max,0}}(1 + M_s), \tag{29}$$

where $T_{\text{max,0}}$ is the maximal tension at baseline, i.e. when the regulatory state M_s is equal to zero. The latter is defined by the following relation

$$M_s = \frac{e^{2M_{s,1}} - 1}{e^{2M_{s,1}} + 1}, \tag{30}$$

where

$$M_{s,1} = G_{\text{myo}} x_{\text{myo}} + G_{\text{meta}} x_{\text{meta}} + x_{\text{baro}} + x_{\text{init}}, \tag{31}$$

where x_i and G_i are the state and gain of the regulation mechanism i and x_{init} is the regulatory state at baseline. The state equations for x_i are described later on. Summarizing, the Laplace law is used to translate a change in regulatory state to a change in arteriolar radius. Actual changes in resistance and compliance of the micro-circulation are derived by coupling the arteriolar radius r_a to the arteriolar resistance R_a and volume C_a via

$$R_a = \frac{K_{a,R}}{r_a^4} \tag{32}$$

and

$$C_a = \frac{K_{a,C} r_a^2}{p_a}, \tag{33}$$

where

- $K_{a,R}$ is chosen such that the baseline arteriolar radius r_a and pressure p_a result in baseline flow q_a. Where baseline means the supine position and $M_{s,1} = x_{\text{init}}$.

- $K_{a,C}$ is chosen such that it corresponds with a total RC-time of $2.0\ [s]$ under baseline conditions.

Summarizing, the arteriolar resistance and compliance are regulated based on the arteriolar radius r_a. The latter is derived from the arteriolar wall tension based on the Laplace law. The muscular tension T_m is the part of the tension affected by the state of the regulation mechanisms x_i. In the following sections the state equations for the three regulation mechanisms are explained.

B.2 Myogenic regulation mechanism

Myogenic regulation protects the micro-vasculature against high pressures by increasing vascular tone upon increasing circumferential stresses and strains. Myogenic activation A_{myo} is therefore based on the current arteriolar tension T_{tot} [Spronck et al., 2012]

$$A_{\text{myo}} = \frac{T_{\text{tot}} - T_{\text{myo,0}}}{T_{\text{myo,s}}}, \tag{34}$$

where $T_{\text{myo,0}}$ is the tension at baseline pressure for $M_{s,1} = x_{\text{init}}$ and $T_{\text{myo,s}} = 0.2T_{\text{max,0}}$ is a normalization tension. The myogenic regulation state x_{myo} is defined by

$$\frac{dx_{\text{myo}}}{dt} = \frac{A_{\text{myo}} - x_{\text{myo}}}{\tau_{\text{myo}}}, \tag{35}$$

where τ_{myo} is the myogenic time constant.

B.3 Metabolic regulation mechanism

Metabolic regulation can be initiated via different metabolites, such as potassium ions, adenosine, lactate and CO_2. These metabolites are generated during a muscle contraction and are washed out by the blood flow. In the current model CO_2 is chosen to be the determining metabolite for the regulation of blood flow during muscle contraction. First, the tissue CO_2-concentration C_{t,CO_2} is defined as the balance between metabolic rate and muscle perfusion q_d

$$\frac{dC_{t,CO_2}}{dt} = \frac{1}{V}\left(M_{CO_2} - q_d\left(C_{v,CO_2} - C_{a,CO_2}\right)\right), \tag{36}$$

where V is an estimate of the perfused muscle tissue volume, C_{v,CO_2} and C_{a,CO_2} are the venous and arterial CO_2-concentration respectively, of which the latter is fixed [Spronck et al., 2012]. The metabolic rate M_{CO_2} is related to muscle activity as follows:

$$M_{CO_2} = M_{CO_2,0}\left(1 + A_{\text{mc}}\left(f_m - 1\right)\right), \tag{37}$$

where f_m is the ratio of metabolic rate at rest and maximal activity and A_{mc} is muscle activity, which is defined to follow the contraction pattern (see Section 2.1.6 for the full definition). Furthermore, $M_{CO_2,0}$ is the basal metabolic production of CO_2 by a tissue of volume V

$$M_{CO_2,0} = M_{CO_2,0,m}\rho_m V, \tag{38}$$

where ρ_m is the muscle density and $M_{CO_2,0,m}$ is the basal metabolic CO_2-production per kg tissue. Muscle perfusion q_d in Equation (36) is the flow leaving the tissue, which is calculated using

$$q_d = \frac{p_2 - p_3}{R_a/2}, \tag{39}$$

where p_2 and p_3 are the pressure at node n_2 and n_3 respectively (Figure 3). Furthermore, C_{v,CO_2} is the venous CO_2-concentration and is determined by the following relation [Irving et al., 1932]

$$C_{v,CO_2} = \alpha_{t,v} C_{t,CO_2} + \beta_{t,v}, \tag{40}$$

where $\alpha_{t,v}$ and $\beta_{t,v}$ are fitting constants. The metabolic activation A_{meta} is determined by the CO_2-concentration in the tissue using

$$A_{\text{meta}} = \frac{C_{\text{t,CO}_2} - C_{\text{t,CO}_2,0}}{C_{\text{t,CO}_2,\text{s}}}, \tag{41}$$

where $C_{\text{t,CO}_2,0}$ is the steady state solution of Equation (36) and $C_{\text{t,CO}_2,\text{s}} = C_{\text{v,CO}_2,0} - C_{\text{a,CO}_2}$ is a scaling term. Finally, the metabolic regulation state x_{meta} is defined by

$$\frac{dx_{\text{meta}}}{dt} = \frac{A_{\text{meta}} - x_{\text{meta}}}{\tau_{\text{meta}}}, \tag{42}$$

where τ_{meta} is the time constant governing metabolic regulation.

B.4 Baroreflex regulation

The baroreflex is a global regulation mechanism which aims to maintain systemic pressure by affecting the heart rate, heart contractility, venous unstressed volume and peripheral resistance. In this study, only the effect of the baroreflex on the peripheral resistance is included, which is based on the model of Ursino [1998] (also implemented in other studies [Lim et al., 2013, van der Hout-van der Jagt et al., 2013]). The carotid pressure p_{carotid} is used as an input parameter and is defined as mean systemic pressure (see Section 2.3 for details) plus a hydrostatic column of 20 cm in tilted position. First, carotid pressure is compared to a reference pressure p_{n}, which is defined as the baseline pressure in the supine position

$$\Delta p_{\text{baro}} = p_{\text{carotid}} - p_{\text{n}}. \tag{43}$$

This pressure difference Δp_{baro} is converted to an afferent baroreflex firing f_{ab} rate via a sigmoidal transfer function

$$f_{\text{ab}} = \frac{f_{\text{ab,min}} + f_{\text{ab,max}} \cdot e^{\left(\frac{\Delta p_{\text{baro}}}{k_{\text{dp}}}\right)}}{1 + e^{\left(\frac{\Delta p_{\text{baro}}}{k_{dp}}\right)}}, \tag{44}$$

where $f_{\text{ab,min}}$ and $f_{\text{ab,max}}$ are the firing rates reached for minimal and maximal Δp_{baro} and k_{dp} is a constant determining the slope of the afferent firing rate. The firing rate for the sympathetic innervation of the peripheral micro-circulation f_{sp} is calculated via the following relation:

$$f_{\text{sp}} = \begin{cases} f_{\text{sp},\infty} + \left(f_{\text{sp},0} - f_{\text{sp},\infty}\right) \cdot e^{-\,k_{\text{es}}\, f_{\text{ab}}} & \text{for } f_{\text{sp}} < f_{\text{sp,max}} \\ f_{\text{sp,max}} & \text{for } f_{\text{sp}} \geq f_{\text{sp,max}} \end{cases}, \tag{45}$$

where k_{es} is a parameter defining the shape of the sympathetic firing rate. The parameters $f_{\text{sp},0}$ and $f_{\text{sp},\infty}$ are the firing rates at zero and infinite afferent firing rate, and $f_{\text{sp,max}}$ is the maximal sympathetic firing rate. The sympathetic innervation is converted to an unfiltered change in resistance ΔR^*

$$\Delta R^* = \begin{cases} G_{\text{R}} \cdot \ln\left(f_{\text{sp}}(t - D_R) - f_{\text{sp,min}} + 1\right) & \text{for } f_{\text{sp}} \geq f_{\text{sp,min}} \\ 0 & \text{for } f_{\text{sp}} < f_{\text{sp,min}} \end{cases}, \tag{46}$$

where G_{R} is a constant gain, D_R is a pure time delay and $f_{\text{sp,min}}$ is the minimal sympathetic firing rate affecting the resistance. The actual change in resistance ΔR is calculated based on ΔR^* using a low pass filter

$$\frac{d\Delta R}{dt} = \frac{1}{\tau_R} \cdot (\Delta R^* - \Delta R)\,, \tag{47}$$

where τ_R is the time constant of the low pass filter. Finally, the relative change in resistance c_{baro} is calculated using the following relation

$$c_{\text{baro}} = \frac{\Delta R - R_{\text{ref}}}{R_{\text{ref,Ursino}}} + 1 = \frac{R_{\text{baro}}}{R_{\text{ref}}}, \tag{48}$$

where R_{ref} is the resistance in baseline conditions in supine position and $R_{\text{ref,Ursino}}$ is the baseline resistance in the model of Ursino [1998]. To combine the baroreflex with the local auto-regulation mechanisms, the resistance is converted into a regulation state x_{baro} similar to the regulation state of the other mechanisms. Firstly, the resistance is converted to arteriolar radius using Equation (32)

$$a_{\text{baro}} = \left(\frac{K_R}{R_{\text{baro}}}\right)^{1/4}. \tag{49}$$

Using Laplace's law (Equation (24)) the arteriolar radius is converted into a change in muscular tension due to the baroreflex

$$T_{\text{m,baro}} = p_{\text{a}} a_{\text{baro}} - T_{\text{e,baro}} - T_{\text{v,baro}}, \tag{50}$$

where $T_{\text{e,baro}}$ and $T_{\text{v,baro}}$ are calculated using $r_a = a_{\text{baro}}$ (Equation (25) and (27) respectively). From the muscular tension the total regulation state $M_{\text{s,baro}}$ is derived using Equation (28) and (29)

$$M_{\text{s,baro}} = \frac{T_{\text{m,baro}}}{T_{\text{max,0}} \cdot e^{-\left(\frac{a_{\text{baro}} - a_{\text{m}}}{a_{\text{t}} - a_{\text{m}}}\right)^n}} - 1. \tag{51}$$

Finally, the total regulation state is converted to the regulation state via Equation (30) and (31)

$$x_{\text{baro}} = M_{\text{s,1,baro}} - x_{\text{init}} = \tanh^{-1}\left(M_{\text{s,baro}}\right) - x_{\text{init}} = \frac{1}{2}\ln\left(\frac{1 + M_{\text{s,baro}}}{1 - M_{\text{s,baro}}}\right) - x_{\text{init}}. \tag{52}$$